IEEE Access
Multidisciplinary ⋮ Rapid Review ⋮ Open Access Journal

Received 1 September 2022, accepted 20 September 2022, date of publication 27 September 2022, date of current version 6 October 2022.

Digital Object Identifier 10.1109/ACCESS.2022.3210348

TOPICAL REVIEW

The Insulation Resilience of Inverter-Fed Low Voltage Traction Machines: Review, Challenges, and Opportunities

TIMO PETRI[1,2], MARINA KELLER[1], AND NEJILA PARSPOUR[2]
[1]Corporate Research, Robert Bosch GmbH, 71272 Renningen, Germany
[2]Institute of Electrical Energy Conversion, University of Stuttgart, 70569 Stuttgart, Germany
Corresponding author: Timo Petri (timo.petri@de.bosch.com)

ABSTRACT The use of wide bandgap (WBG) semiconductor devices, which enable higher switching slew rates, and the increase in DC link voltage, which provides system-wide advantages, exposes the winding system of traction machines to enhanced electrical stress. The resulting nonlinear voltage distribution along the motor winding favors partial discharges (PD), which in low voltage (LV) machines causes excessive damage to the insulation system, and premature failure can occur. A simple solution by increasing the enamel thickness of the wires leads on the one hand to a lower copper fill factor. On the other hand, this measure is not necessarily accompanied by an increase in electrical resilience in the case of pulsed voltage. It is therefore essential to understand the phenomenon of partial discharges, which is composed of a large number of processes and mechanisms, to be able to make an estimation of aging. The ultimate goal is to derive a lifetime model that links the dynamic load collectives – ideally in conjunction with the environmental stress influences – of a traction application to a usage-dependent and realistic prediction of the residual lifetime. To this end, this paper provides an overview of the current state of science and technology in this interdisciplinary topic by describing, with reference to high voltage (HV) technology/engineering, the design of the insulation system, the discharge physics, the degradation mechanisms, the statistical effects to be considered, and the partial discharge measurement methods.

INDEX TERMS Accelerated aging, automotive, electrical machine, electrical stress, hairpin, insulation degradation, insulation system, partial discharge, pulsed voltage, SiC inverter.

I. INTRODUCTION

In the course of the electrification of the transport sector, the interaction of the inverter and the electric machine, connected via cable (Fig. 1), will play a decisive role in future traction drives in terms of holistic system efficiency, costs, and reliability [1]. In battery electric vehicles (BEV), the battery is the most expensive system component. So the conflicting optimizing goals for the manufacturer are to keep it as small as possible while maximizing the usable energy content for a high practical driving range of the BEV [1]. This is achieved by increasing the efficiency of the powertrain. Due to technological advances in power electronics, there are mainly two trends, that increase system efficiency, but also affect the motor insulation resilience: increasing the switching slew rate or the voltage gradient $\mathrm{d}v/\mathrm{d}t$ (Section I-A) and increasing the DC link voltage U_{DC} (Section I-B) [2].

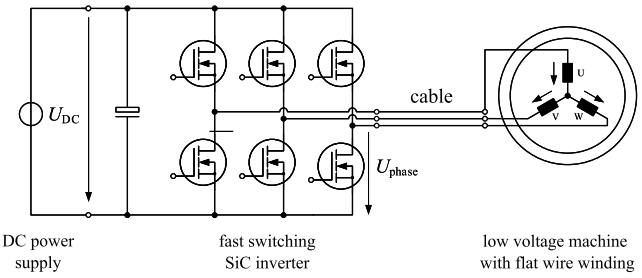

FIGURE 1. System overview.

The associate editor coordinating the review of this manuscript and approving it for publication was Xiaodong Liang.

It has been known for a long time that an inverter feed causes increased electrical stress on the insulation system of low voltage (LV) machines due to repetitive voltage impulses, which are inherent in their principle. In this regard, it is a kind of renaissance of the phenomenon compared to the introduction of the insulated gate bipolar transistor (IGBT) devices [3], [4], [5]. However, the electrical stress is further increased by the two factors mentioned and the reliability decreases significantly if no countermeasures or fundamental system changes are made, which increases electrical resilience [6]. In addition to the electrical stress, the electric machine is exposed to further multifactorial interacting influences during operation – the so-called TEAM factors (thermal, electrical, ambient, mechanical). They contribute to the machine's aging, which means they worsen irreversibly its thermal, mechanical and electromagnetic characteristics and lead in the worst case to total failure.

The focus of this article is on electrical stress, where a complex cause-and-effect relationship exists between the influencing factors, making it challenging to model the physical behavior in total. The content of this article will be limited to the aging effects in the stator winding, as this is the most common electrically induced cause of failure in standard industrial motors [7], [8], [9]. For this purpose, the phenomenon of partial discharge (PD) and the physics behind it are examined in more detail. As the scope of this article addresses the automotive industry with its high production volumes, cost-saving issues play a major role also for the insulation system design. This is why well-established technologies, methods, and materials from the HV sector cannot be applied in a straightforward manner. High safety margins or alternative materials are simply too expensive or not suitable for BEVs. Hence, a profound understanding is required, for designing the insulation system to the edge, avoiding cost-intensive over-engineering, as is still the practice at the moment [6]. Unfortunately, those required insights are currently not at hand, which will be outlined throughout this paper.

A. INCREASING THE SWITCHING SLEW RATE

On the inverter side, fast switching wide bandgap (WBG) semiconductor devices, namely silicon carbide (SiC) metal oxide semiconductor field effect transistors (MOSFETs), offer better electrical and thermal properties: lower conduction and switching losses and higher thermal conductivity. Using state-of-the-art silicon based insulated-gate bipolar transistors (Si-IGBT) with switching slew rates $\mathrm{d}v/\mathrm{d}t$ of around $10\,\mathrm{kV}/\mu\mathrm{s}$, the new SiC MOSFETs can achieve switching slew rates of over $100\,\mathrm{kV}/\mu\mathrm{s}$. As a result, the switching frequency can also be increased, which leads to a smaller current ripple in the motor and consequently to less pulse width modulation (PWM) related additional losses. Further system advantages result from the increase of the DC link voltage from 400 V to 800 V systems. But these advantages come at the price of higher electrical stress on the machine side. The high $\mathrm{d}v/\mathrm{d}t$, the discontinuous transmission line consisting of inverter, cable connection, and electric machine as well as resonance phenomena cause voltage overshoots and high frequency oscillations at the motor terminals, which stress the winding insulation with even more than the DC link voltage. Due to wave propagation effects, there is a highly nonlinear voltage distribution along the motor winding and higher potential differences between the conductors are possible [10], [11], [12], [13], [14], [15], [16].

B. INCREASING THE DC LINK VOLTAGE

The 400 V systems, resulting in 150 V – 400 V DC link voltage, have since become established as the automotive standard when considering the currently available EV [17]. This is mainly due to the commercially available large numbers of IGBT power semiconductors with a voltage class of 600 V and the fact that the switching losses with Si-IGBT would increase too much with higher DC link voltage. The voltage class is defined by the maximum permissible reverse voltage and a certain safety margin is necessary with respect to the DC link voltage due to the voltage peak that occurs during the switch-off process [18]. The advantage of the 800 V systems (DC link voltage up to 870 V) is that, for the same required power, the currents are halved accordingly and thus also the conductor cross-section. The electrical system advantages include a reduction in the semiconductor area, which is linked to the cooling effort, and electrical contact areas and lower copper losses. From a design point of view, this results in advantages in the form of reduced wire bending radii between the HV system components and a reduced installation space as well as material and weight savings. Ultimately, a further gain is a reduction in charging times, as the EV can be charged at higher powers (> 200 kW) [17].

C. CONTRIBUTION

The article is primarily aimed at engineers and scientists who would like to gain an overview of the interdisciplinary field of insulation management of inverter-fed LV traction motors, which recently attracted much attention. For this purpose, relevant primary literature was analyzed in depth and is referenced accordingly in this paper. The factors that influence the aging of the machine are identified. Physical processes and cause-and-effect relationships associated with aging are presented for a basic understanding. PDs are regarded and the state-of-the-art of lifetime estimations is outlined. Further, it is pointed out that the hairpin winding type warrants further research efforts. Measurement techniques and statistics, which are also associated with difficulties in this context, are addressed. All as a whole, the article was written with reference to high voltage (HV) technology/engineering in a comparative and classifying form.

II. DESIGN OF THE ELECTRICAL INSULATION SYSTEM OF ROTATING MACHINES AND REFERENCE TO HIGH VOLTAGE TECHNOLOGY/ENGINEERING

This section establishes the reference to HV technology/engineering. By showing the differences in the design of HV machines, it becomes apparent why recently increasing

problems in the insulation system of inverter-fed LV machines were reported and that so far no solution and understanding have emerged.

Insulation systems have been the core of HV technology ever since and enable the control of high voltages and high electric field strengths [19], [20]. For the resilience of an insulation system, the level of the occurring electric field strength E is determining, which has the following integral relationship with the voltage in the electrostatics:

$$U_{12} = \Delta\varphi_{12} = \int_{x_1}^{x_2} \vec{E}\,\mathrm{d}\vec{s} \tag{1}$$

With U_{12} the voltage over a distance x_1 to x_2 and $\Delta\varphi_{12}$ being the electrical potential difference between those two points. And in the presence of a uniform field, with $x_1 = 0$ and $x_2 = d$ simplifies to:

$$U = E \cdot d \tag{2}$$

In the HV technology field, voltages $> 1000\,\mathrm{V_{RMS}}$ are applied with usually large to very large machine/device dimensions at the same time, which is also reflected in the insulation path length. Inherent to the traction drive in the automotive sector is that it must meet the requirement of high power density. If the power density is to be increased within the same available construction space, which is indirectly defined by the conductor cross-sections of the windings, the rated voltage level must increase. Consequently, the electric field strengths in the motor increase. The problem is intensified by undesirable transient voltage peaks as a result of voltage reflections that occur during fast switching in inverter operation. In energy technology, a main field of application of HV technology, HV motors and generators mainly operate stationary at the three-phase 50 or 60 Hz power grid under constant ambient conditions. However, there are also applications in HV technology where stress is applied with surge voltages and fast-rising pulses. So, the topic is not foreign in the HV field.

One principle of HV technology is that the electrical stress due to the surge characteristic can be increased if the stress time is reduced [19]. Accordingly, at a high $\mathrm{d}v/\mathrm{d}t$, an increase in stress would be possible. Furthermore, the phenomenon of PD in HV technology, e.g. in gas-insulated substations (GIS), has been the subject of intensive research for several decades [21]. For pulse capacitors in HV technology, the lifetime is determined by the transient stress during discharge, and the systemic circuit damping of the capacitor has a significant influence [19]. Therefore, the load-dependent oscillation and decay behavior in terms of the wave effects at the motor terminals should be included in the consideration as an aging influencing factor of the machine insulation system.

The design of an electric motor is usually based on quasi-stationary conditions. Consequently, the displacement current is neglected and accordingly the modeling is limited to an inductive-resistive system. The nonlinear character of magnetic materials, given by the magnetization curves, must be taken into account. In HV technology, mainly the electric field strengths in insulation systems, such as for HV cables for energy distribution, are investigated and represented accordingly in models. Here quasi-stationary conditions are also used for modeling, but in these models, the displacement current predominates over the conduction current due to the low residual conductivity of the insulation. This results in a contrary capacitive-resistive modeling approach. Dielectric materials behave linearly at moderate frequencies, so the superposition principle can be applied when considering stress. Transmission line conducted waves tend to be of secondary importance in HV technology and must be considered for extended systems like underground cables or overhead power lines and for special systems with fast-rising pulses [19].

A. CONSTRUCTIVE MACHINE DESIGN

Considering the variety of HV machines developed and produced in the past, it can be seen that they had one thing in common [22]. They were usually designed very conservatively to guarantee the longest possible lifetime (20 – 40 years) [23]. In fact, many machines from the early 1900s are still in use [22]. Improvements in many areas, such as manufacturing and in the materials used, as well as computer-aided design through dedicated software tools, have enabled the stress to increase steadily since then [22]. Nevertheless, classical HV machines are operated at comparatively low voltages ($< 27\,\mathrm{kV}$) in relation to their high electrical power (up to 2 GVA [23]), which is also the reason for their enormous size. This is because large rated power requires large conductor cross-sections for conducting these high currents. The reason for limiting the voltage is that no further increase in electrical resilience is possible above a certain insulation thickness [19].

1) CLASSIFICATION

In literature, depending on the source, two or three types of stator windings are classified, with the latter two then being understood as one type of winding [23]:

- random wound windings (round wire windings)
- form wound windings (flat wire windings with multiturn coils)
- Roebel bar windings (flat wire windings with several parallel bars in a special arrangement for suppressing high eddy current losses)

Further classifications, e.g. according to winding head design and winding manufacture, are also established [24], [25], [26]. Round wire windings are used up to a voltage of $1000\,\mathrm{V_{RMS}}$. The upper limit of the power spectrum is thus limited to a few 100 kW. LV machines in the industrial environment are usually designed with round wire windings. An exception is a new development in the automotive field, where flat wire windings, also known as hairpin and I-pin windings, are increasingly used (see Section II-A2). Flat wire windings are otherwise only used for motors and generators with higher power ratings, and Roebel bar windings are

only used for very large generators. For power ratings above 500 MVA, the Roebel bars are sometimes designed as hollow conductors for the purpose of direct water cooling [23].

According to the standard IEC 60034-18-41 [27], two types of insulation systems are distinguished:

- Type I: $< 700\,V_{RMS}$, PD-free (over lifetime)
- Type II: $> 700\,V_{RMS}$, PD-resistant

Thus, the standard does not coincide with the conventional transition from LV to HV machines at $1000\,V_{RMS}$ [28], [29]. Since the definition of type II means that PD (see Section III) can occur, this has a significant effect on the design and materials used for insulation.

2) HairPIN/I-PIN TECHNOLOGY

Normally, exclusively random wound windings are used in the LV range, but in the automotive industry with its special requirements, such as small available construction space and high power density, hairpin windings are more advantageous for the following reasons [2], [30], [31], [32]:

- high copper fill factor
- as a result, higher phase currents are possible, which allow higher torque
- improved heat transfer between winding and stator slot
- good mechanical properties such as high rigidity
- production with a high degree of automation
- cost efficiency due to a high degree of scalability
- high potential for improvement in production technology

B. ELECTRICAL INSULATION SYSTEM AND MATERIALS OF LV AND HV MACHINES

With the insulation system, which is a passive component of the stator in contrast to the copper conductors and the highly permeable stator laminations, a differentiation is made between primary and secondary insulation. The primary insulation is classified according to function as phase-to-ground, phase-to-phase and turn-to-turn insulation. The impregnation in the form of resin or varnish represents the secondary insulation [33], [34], [35]. The materials used for Type I according to the standard [27] are nowadays (high) temperature resistant polymers, whereby the primary insulation is organic thermoplastics and the secondary insulation is organic thermosets. Inorganic materials, such as porcelain, glass, and mica, which are characterized by their high resistance to chemical and environmental influences, excellent thermal properties, and PD-resistance, are reserved for type II insulation systems.

The materials used also depend on the thermal stress and the associated design of the machine. Hence, electrical insulation materials (EIM) or electrical insulation systems (EIS) are classified according to the standard IEC 60085 [36] into a thermal class, which corresponds to the maximum service temperature. In connection with thermal properties, the temperature index (TI) from standard IEC 60216-1 [37] and standard IEC 60317-0-1 [38] should also be mentioned, which establishes a relationship between the operating temperature and the thermal aging of the EIS or EIM with the aid of test procedures.

A number of different cooling methods exist, which differ in terms of the arrangement and number of cooling circuits, the coolant used, and the type of movement of the coolant [39], [40]. In principle, a distinction is made between indirect and direct winding cooling. With direct cooling, the coolant flows through hollow conductors, inserted tubes or channels within the main insulation. A further distinction is made between gas and liquid cooling. Gas cooling is realized with air or hydrogen and liquid cooling mainly with water, rarely with oil [24]. Traction machines mostly have liquid cooling in the form of a cooling jacket integrated into the housing, air cooling is also possible [41]. Industrial motors usually have a self-fan on the shaft, which is speed-dependent. Large turbo generators are cooled with hydrogen [24], [42].

1) LV MACHINES ($< 700\,V_{RMS}$ [27] OR $< 1000\,V_{RMS}$ [28])

The extensive range of applications for electrical machines results in correspondingly different requirements for the machine design, which is equally reflected in a variety of different insulation materials and the associated manufacturing processes [26]. The enamel insulation is applied to the copper wire in several steps. The number of layers determines the grade (G1 – G3) of the insulation. The thickness of the coating layer increases as the conductor cross-section increases. In the available articles diameters between 0.25 – 3.0 mm with grade 2 or 3 can be found. Mostly grade 2 wire pairs with a diameter of 0.5 mm or 1.0 mm and an insulation layer between approximately 30 – 40 µm are used [43], [44], [45], [46], [47]. The enamel layers for hairpin windings can be 50 – 200 µm, typical is 80 µm like our exemplary investigated machine [2]. The requirements for the enameled wire can be found in the standard IEC 60317-0-1 [38] and are verified to be met by the procedures described in the standard IEC 60851-5 [48]. Polyimide (PI), polyamide-imide (PAI), (tris-2-hydroxyethyl isocyanurate modified-) polyetherimide ((THEIC-) PEI), (THEIC-) polyesterimide ((THEIC-) PESI) can be used as a basecoat and polyaryletherketone (PAEK) or polyetheretherketone (PEEK) as a overcoat [33], [49], [50]. In addition to the enamel of the conductors, the primary insulation also includes the slot liner and phase separator in the slot as well as in the winding head, which can also be realized with a variety of materials in LV machines. Usually, these consist of discrete individual materials such as paper, foils, or multilayer composite materials such as flexible laminates and have a thickness of 100 – 300 µm [33], [50]. Some of these can also absorb small amounts of resin. The slot liner of hairpin windings is designed as an S-, B-, or U-shape [31]. Stiffer materials, such as rigid laminates, are used for wedges in the slot liner because of their higher mechanical strength. For flexible laminates, a two- or three-layer combination of the following materials is used: cotton paper, aramide paper, polyester film/nonwoven, and polyimide film [33], [50].

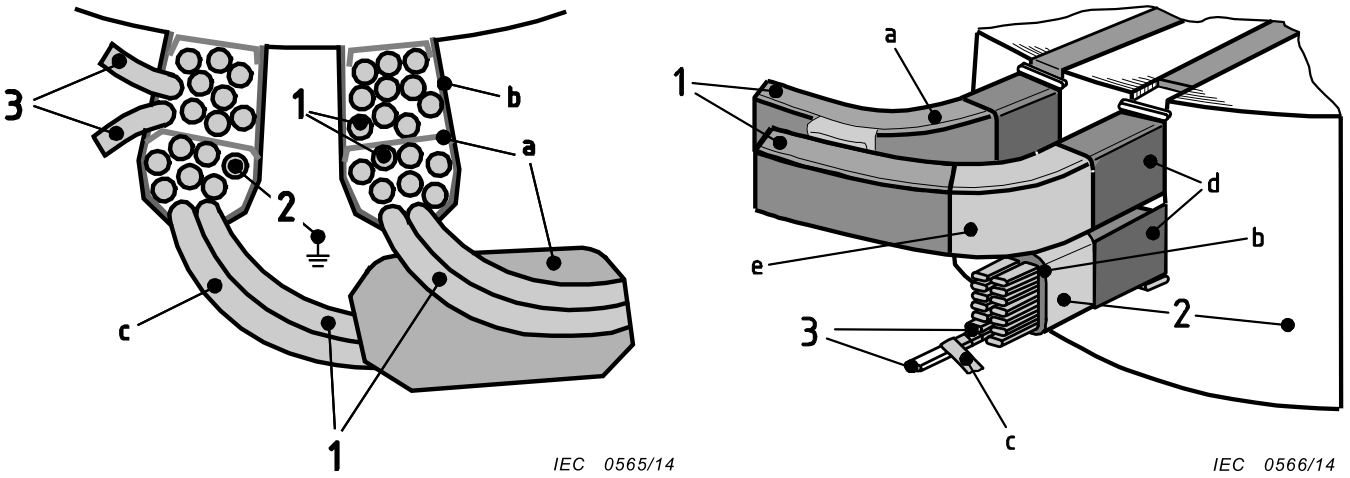

(a) Random wound machine (b) Form wound machine

FIGURE 2. **Main components of the insulation system for: (a) LV machines, (b) HV machines. Labeling: 1 phase to phase, 2 phase to ground, 3 turn to turn, a phase insulation/overhang insulation, b mainwall insulation, c turn insulation, d slot corona protection, e overhang corona protection (stress grading) [27].**

The materials used in secondary insulation in the form of impregnating varnishes or resins, which also improve mechanical strength and heat dissipation, are based on polyesters, epoxies, and polyesterimide [33], [50]. There are three manufacturing processes for impregnation that affect the insulation quality and therefore the electrical resilience: dip impregnation, trickle impregnation, and (global) vacuum pressure impregnation (VPI) [23], [33], [50].

2) HV MACHINES ($> 700\,V_{RMS}$ [27] OR $> 1000\,V_{RMS}$ [28])

HV machines differ fundamentally in their design and choice of materials. The subconductor insulation consists either of a polymer varnish or, as shown in Fig. 2b, of thin mica tapes or foils with which the subconductor is wound [19], [23], [51]. Mica is a naturally occurring inorganic material that is characterized by its high resilience to PDs and it prevents the erosion effect of PD [52], [53]. Due to this resilience, even PDs of high magnitude are considered uncritical in HV machines, therefore changes in PD activity are used as an indicator of aging in the course of PD monitoring, which is intended to prevent premature machine failures. In LV machines, the occurrence of partial discharges leads to a rapid premature failure of the machine. Between the windings and the laminated core lies the main(wall) insulation, which has an inner and outer corona (see Section III) protection in the form of a conductive layer. The inner corona protection serves to make the electric field strength uniform and the outer corona protection, which lies on the potential of the stack of laminations, prevents slot discharges in possible cavities [19], [23], [54]. In addition, the field strength enhancement at the endpoints of the bars leaving the slot is suppressed by the overhang corona protection, a form of field control. This consists of semiconducting (nonlinear) materials that reduce the potential gradually in the longitudinal direction and thus prevent surface discharges (see Section III) [19]. Polyester, polyesterimide epoxy, and silicone-based resins are also used for secondary insulation, but with difference from LV machines is the tapes highly absorb the resin [53], [55]. The possible application processes are VPI and resin-rich (RR) impregnation, in which the tapes already contain the resin before being wrapped [23], [53], [55]. The insulation thickness moves further into the millimeter range as the rated power of the machine increases [53].

III. PHYSICAL MODELING

This section will briefly outline the physical relationships in the context of insulation systems. Fig. 3 is intended to give an overview with the help of a schematic structure showing the relations between relevant domains of the insulation system of electrical machines. The focus is limited to the electrical and electrically induced stress and the associated relationships.

In Fig. 3 the designations in the bubbles of the schematic illustration represent a generic term for the respective domain. The sum of the domains on the left side forms the insulation system of the electrical machine as it physically exists. On the right side, the domains are shown that are supposed to represent the insulation system through known property values, physical and chemical modeling, calculation, and a possible verification through tests.

The domain ''geometry and medium'' subsumes the geometric description and the chemical material properties. The specific mechanical arrangement and the dielectric properties of the insulation section in the dedicated insulation system are the basis of every investigation. The domain ''electrical stress'' is primarily characterized by the voltage signal in time. Secondary are the current parameters. Electrical stress is represented by stress factors such as the voltage level, switching frequency, etc. The basic approach depends on the type of insulation system. The fundamental approach

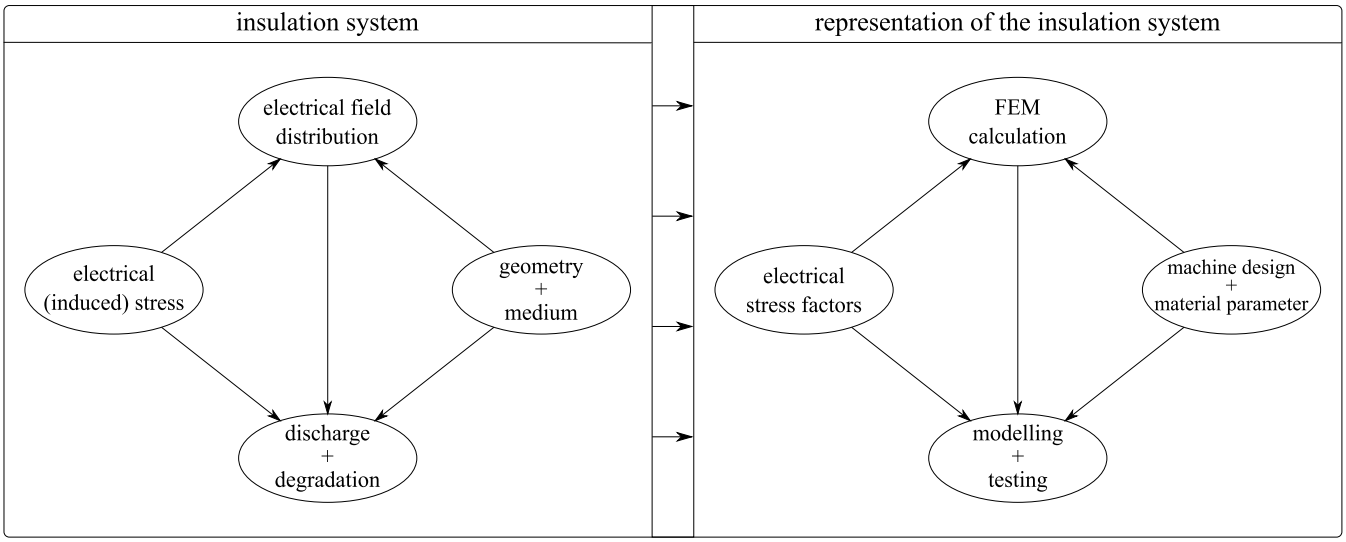

FIGURE 3. The relational structure of the domains of the insulation system and its representation.

depends on the voltage type (AC, DC, pulsed voltage (PV), mixed (M) voltage). The stress duration or frequency is a further major parameter. In terms of ''field distribution'', the uniformity of the field is of decisive importance, as well as the possible presence of surface or space charges. They determine the discharge mechanism and the maximum stress occurring in the insulation system. The physical description of the discharge behavior and the associated damage mechanism is assigned to the domain ''discharge and degradation''. There are different forms of discharge. The discharge behavior is the criterion for assessing the electrical resilience of an insulation system, as resilience and reliability are derived from it. In Table 1, the representation of the domains is broken down in detail to their constitutive quantities, which influence the discharge behavior.

The degree of electrical resilience depends on the material composition and arrangement of the insulation path. Insulation paths with gas (e.g., air, sulfur hexafluoride (SF_6)) as insulation medium have the lowest electrical resilience. Insulation systems with sections under vacuum have higher resilience. Liquid (e.g., mineral oil for transformers) and solid insulating materials (e.g., paper, epoxy resin) are used when the resilience of the gases or liquids is not sufficient or mechanical requirements have to be met [19]. When choosing a medium, the advantages and disadvantages it brings must be weighed against each other for the specific application. A distinction must be made between theoretical and technically usable resilience. Thus, solid materials in ideal form have a higher resilience than gaseous materials, but the technically usable resilience can even be below this [56]. In this consequence, the individual manufacturing influences and conditions of use have a greater influence than the physical material properties [19]. The specific causes are discussed in Section IV-A.

If the electric field strength in an insulation system exceeds a critical level in a partial area of the insulation section (nonuniform case), discharges – so-called partial discharges (PD) – can occur in this area. This means that a complete breakdown does not occur, as would be the case with uniform field distribution. The insulation remains intact. A distinction is made between internal and external PDs, the latter also known as corona discharges. Internal PDs occur in (micro-) cavities in solid mediums.

To evaluate the resilience of an insulation system of a rotating electrical machine, the discharge behavior must be investigated. Therefore, the established physical models of discharges are described in this chapter. Wherever an electric field is present in the insulation system and gas (e.g., air) is the insulation medium, gas discharges can occur. The same applies to imitations of insulation systems such as wire pairs. Regarding these abstract physical models, the concrete sources from which gas discharges can originate are found in Section IV-A4. In addition, there are areas in the insulation system of the machine where an electric field is present in a solid medium, such as impregnation resin. The medium can be composed of several layers, where these can also be filled with gas. Since discharges can occur in solid mediums or multilayer mediums, this is as well described in this chapter.

A. STATIC DESCRIPTION OF GAS DISCHARGES

In contrast to solid and liquid insulating materials, the discharge mechanisms of gases can be described by a comprehensive physical theory because of their well-defined properties [19]. In the case of gas discharges, a distinction is first made between self-sustaining and nonself-sustaining discharges. It is called a nonself-sustaining discharge if, when the electric field is applied, the free electrons, which are present in the gas volume due to thermo- and photoionization, cannot ionize neutral gas molecules during their acceleration, whereby further free charge carriers would be available, which would contribute to the current flow [19], [20].

TABLE 1. The schematic domain relation structure broken down in detail.

domain	category	properties	characteristics/variations	quantities
geometry + medium	medium	aggregate state	solid, liquid, gas	density ρ, pressure p, temperature T, Volume V
		chemical composition	organic, inorganic	cathode material, permittivity ε_r, chemical elements, chemical formula, electron affinity
	geometry	machine design	machine type, winding type, cooling type	dimensions, supply cable length l_cable
		insulation system design	insulation components, discrete insulation path	electrode distance d
	geometry + medium	electrical system description	inductive-resistive, capacitive-resistive	impedance Z, characteristic impedance Z_0, frequency response
stress	voltage	type	AC, DC, PV, M	magnitude/amplitude $\hat{U}$, (switching) frequency $f_{(\mathrm{sw})}$
		magnitude/amplitude	steady state, transient, peak	magnitude/amplitude $\hat{U}$, peak voltage U_pk
		form	ideal, not ideal, triangle, square, surge	overshoot OF, damping constant δ, oscillation frequency ω, form equation
	time	stress time	continuous, intermittent	duty cycle D, breakdown delay t_D, probability for start electron F_s, voltage-time area A_s
		rate of change	static, quasi-static, harmonic, dynamic	derivative $\frac{\mathrm{d}}{\mathrm{d}t}$
	current	magnitude/amplitude	no additional heat, additional heat	magnitude/amplitude $\hat{I}$, temperature ΔT
field distribution	field distribution	degree of uniformity	uniform, nonuniform, highly nonuniform	Schwaiger's utilization factor η_s
		space charge	space charge free, space charge affected	charge carrier density n_i
		field strength	background electric field, field enhancement	critical field strength E_crit, background field strength E_0, enhanced field strength E_ef
discharge + degradation	discharge	discharge physics	Townsend, Streamer, DBD, plasma	$\gamma, \alpha, \eta, A, B, \nu_{st}, \lambda_m, \lambda_\mathrm{i}, \lambda_\mathrm{a}, W_\mathrm{i}, W_\mathrm{e}, N_\mathrm{e}$
		discharge form	breakdown, internal PD, corona PD, surface PD	PDIV, PDEV, (see also Table 4)
	degradation	degradation mechanism	erosion, electrical treeing, overstress, heat	PD pulse count m, PD magnitude U_m, apparent charge q, (see also Table 4)

Discharge quantities: γ = feedback coefficient, α = ionization coefficient , η = attachment coefficient, A, B = empirical gas constants, ν_st = streamer propagation velocity, λ_m = mean free path length, λ_i = path length for ionization, λ_a = path length for attachment, W_i = required ionization energy, W_e = required work for electron emission from cathode, N_e = number of electrons

According to the law of conservation of momentum, the velocity of the light electrons barely decreases during the eccentric elastic collision with the heavy gas molecules [19]. The small current flowing through the gas is proportional to the applied voltage and thus exhibits ohmic behavior. Thermoionization or thermoemission occurs only at higher temperatures and is therefore not considered further. At photoionization, a gas molecule is ionized by photons of cosmic radiation or ultraviolet (UV) radiation. Photons can also release electrons from the cathode material, the photoemission. With increasing field strength, a saturation current is established. In addition to photoionization, collision ionization, where additional charge carriers are generated, can occur if the field strength is further increased and the kinetic energy of the accelerated electrons is consequently also higher. When the ignition/inception voltage U_i is reached, these additional charge carriers cause an increase in current, which leads directly to a breakdown in the case of uniform field conditions ($U_\mathrm{i} = U_\mathrm{B}$) and PDs in the case of nonuniform field distribution in the critically stressed gas volume ($U_\mathrm{i} < U_\mathrm{B}$). The electric breakdown is related to the voltage collapse, in the case of PDs a stable operating point is established, which is linked to the well-known luminous phenomena (corona discharges) [19], [20].

B. GENERATION MECHANISM ACCORDING TO TOWNSEND (SPACE CHARGE FREE)

Townsend's theory [57] assumes a uniform and space charge-free Laplace electric field. The generation mechanism starts with the so-called start or initial electron being released

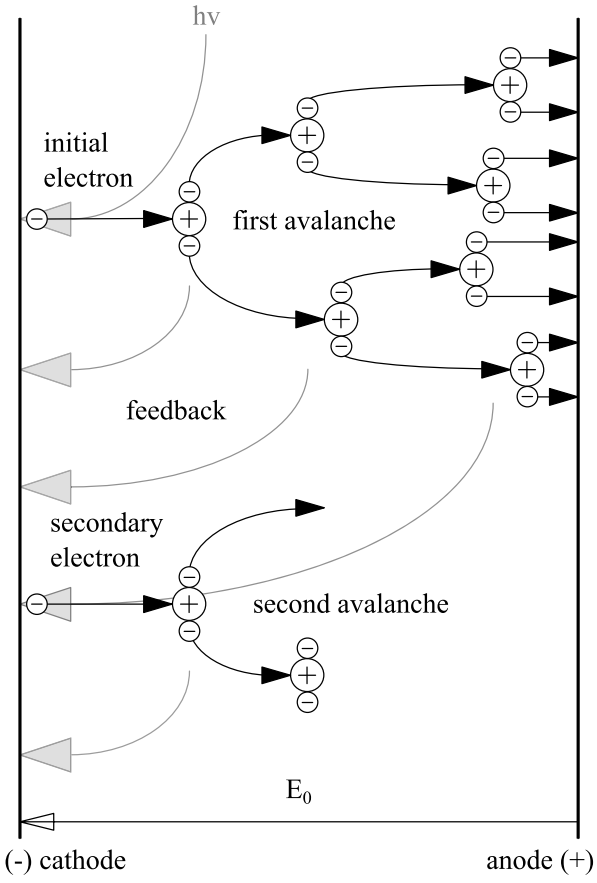

FIGURE 4. Schematic illustration of the process of an electron avalanche (photon energy hν). Adapted from [19].

from the cathode when the required emission energy W_e, which depends on the cathode material, is applied to the electron. In addition to photoemission, field emission, which can be explained by the quantum mechanical tunnel effect and can also occur at lower field strengths for a certain surface roughness, can start the process and release electrons from the cathode (see Fig. 4). When the starting electron is accelerated, the energy is accumulated until the ionization energy is sufficient. The additional electrons created are also accelerated and ionize more gas molecules, starting an avalanche-like process. Positive ions remain, slowly drifting towards the cathode, which can then release electrons from the cathode – the secondary electrons – upon collision. This feedback effect will then trigger an avalanche of follow-on electrons. A conductive path is formed and the voltage collapses. The process can also stop prematurely if not enough secondary electrons are released from the cathode. Mathematically, the ignition condition is defined in general terms for uniform and nonuniform fields at path length d as follows:

$$\int_{x=0}^{d} \alpha_e \, \mathrm{d}x \geq \ln\left(1+\gamma^{-1}\right) = k_g \tag{3}$$

In this, γ is the feedback coefficient (2nd Townsend coefficient), which combines the previous processes into a scalar function of field strength and pressure (see (4)). In addition to the dependence on the cathode material, the gas composition also has an influence on this. k_g is thus the system constant that results for this specific conditions. To the already described ionization processes of emission by positive ions (I), photoemission (P), field emission (F), photoionization in the gas volume by radiation (V) and collision ionization of neutral atoms (N), the ion emission from the anode (A) is considered in the feedback coefficient.

$$\gamma = \gamma_I + \gamma_P + \gamma_N + \gamma_A + \gamma_F + \gamma_V = f\,(E/p) \tag{4}$$

The effective ionization coefficient α_e gives the number of additional electrons generated by an electron relative to the path length x traveled and must be greater than zero for avalanche formation. It is composed of the difference of the ionization (i) coefficient α (1st Townsend coefficient) and the attachment (a) coefficient η, which must be considered for gases with high electron affinity [19]. The effective ionization coefficient α_e, like the feedback coefficient γ, depends on the field strength and pressure and is also a random quantity that is the product of the ionization probability and the collision probability, both of which depend on the mean free path length λ_m. The mean free path length describes the path that an electron travels on average between two collisions and can be expressed with the ionization probability via the Clausius mean path length law [19], [20], [58]:

$$\begin{aligned}\alpha_e = \alpha - \eta &= \frac{1}{\lambda_m}\left(e^{-\frac{\lambda_i}{\lambda_m}} - \left(1 - e^{-\frac{\lambda_a}{\lambda_m}}\right)\right) \\ &= p\left(A \cdot e^{-\frac{B}{E/p}} - \left(a\left(1 - e^{-\frac{b}{E/p}}\right)\right)\right) = p \cdot f\,(E/p)\end{aligned} \tag{5}$$

where $\alpha > \eta$ and zero otherwise. The gas constants a, A, b, and B are determined by experiments. The effective ionization coefficient α_e is then given as a function of field strength and pressure. At this point, it should be pointed out that extensive simplifications have been assumed, which will not be further discussed here.

C. PASCHEN's LAW (SPACE CHARGE FREE)

Before Townsend described the discharge mechanism physically, the empirical relationship between breakdown voltage and the product of pressure p and electrode distance d was established by Paschen [59]. Paschen varied the electrode distances between 0.1 cm and 1.0 cm with electrode spheres ($r = 1.0$ cm, weakly nonuniform field distribution, made of brass) at pressures of 26.67 mbar and 1.0 bar [60]. The Paschen curves in principle have the characteristic shape as can be seen in Fig. 5. At low and high pd-values, the breakdown voltage increases, with the Paschen minimum in between. Below the curve, no gas breakdown is possible. The

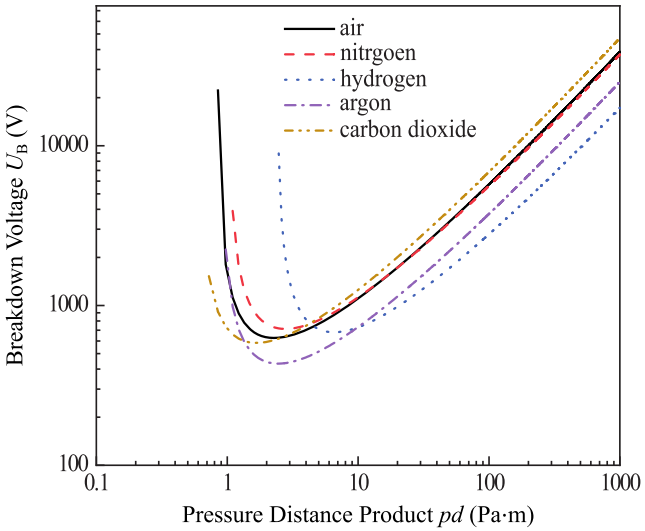

FIGURE 5. Breakdown Paschen curves for different gases. Adapted from [61].

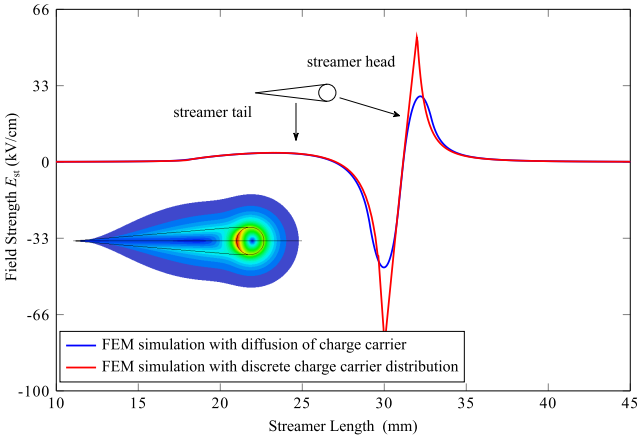

FIGURE 6. Superelevation of the background field due to the space charge in the streamer. Adapted from [69].

exact shape of the curves is not only highly dependent on the gas but also on the cathode material.

Assuming a uniform field, negligible attachment, a constant feedback coefficient, and the limit case consideration, (3) can be formulated with (5) as:

$$(pd) \cdot f\,(E/p) = \ln\left(1 + \gamma^{-1}\right) \tag{6}$$

With the similarity law, (6), and (2) an analytical approximation expression is obtained, which is known as Paschen's law:

$$U_{\mathrm{B}} = \frac{(B \cdot p \cdot d)}{\ln\left(A \cdot p \cdot d\right) - \ln\left(\ln\left(1 + \gamma^{-1}\right)\right)} \tag{7}$$

Paschen's law is used in a large number of publications [3], [45], [46], [56], [62], [63], [64], [65], [66], [67] related to PDs, whereas the conditions are significantly different for the insulation issue of LV machines discussed here. The electric field is (strongly) nonuniform, there are no (quasi-) steady-state conditions, and the electrodes are also coated with polymeric enamel. Paschen's law at this point is taken as a base for calculating the PD inception voltage (PDIV) [45], [46], [56], some papers also deal with the modification of Paschen's law in the presence of other influencing factors such as temperature or humidity [46], [68]. This further implies that space charges, as they occur in the streamer mechanism, are excluded from the consideration.

D. STREAMER MECHANISM ACCORDING TO RAETHER (SPACE CHARGE AFFECTED)

The theory according to Townsend assumes that electron avalanches do not deform the electric Laplace field and therefore no space charge occurs. The assumption is justified below an electron number of about $N_{\mathrm{crit}} = 10^8$ electrons. Above that level, the background field experiences a superelevation due to the space charge. As in the Townsend mechanism, the avalanche process starts with a start electron, with the difference that the start electron occurs in the gas volume or is released from the cathode. Therefore, a distinction is made between cathode-directed and anode-directed streamers. The avalanche consists of a negative spherical avalanche head, where a high space charge density of electrons prevails, and a positive conical avalanche tail, which is formed by the remaining comparatively immobile ions (see Fig. 6). At the front of the streamer, the field strength becomes maximal and the collision ionization and recombination processes, in which photons are emitted (photoionization), increase. Photoionization creates ahead and behind the streamer head avalanches that form a conductive streamer channel. Unlike the Townsend mechanism, where multiple avalanches are required for a breakdown, photoionization in the channel mechanism allows a breakdown to occur via a single avalanche. The left side of Raether's [70] equation is identical to the ignition condition of Townsend's. The right side, which may also be expressed with the streamer system constant k_{st}, differs as can be seen:

$$\int_{x=0}^{d} \alpha_{\mathrm{e}}\,\mathrm{d}x \geq \ln\{N_{\mathrm{crit}}\} = k_{\mathrm{st}} \tag{8}$$

The equation is also valid for nonuniform field distribution, but different ratios of ionization and attachment result in the field regions. In the strongly stressed field Ω the ionization $\alpha > \eta$ predominates, whereas in field-weak areas the attachment $\alpha < \eta$ does. This is schematically illustrated in Fig. 7. In the region Γ_{cr} the ignition condition according to (8) is fulfilled and streamers can be formed in this region. The streamer grows out of the region Ω into the region Ω_{st} because the voltage drop per length after the inception of the streamer is smaller than $U_\Omega = \int_0^{x_\Omega} E\mathrm{d}x$ and can stabilize in this region.

Shown in Fig. 8 are four in HV technology established arrangements consisting of a combination of plate, tip, rod, and sphere, and produce different degrees of nonuniform electric field distribution. For example, Schwaiger found in

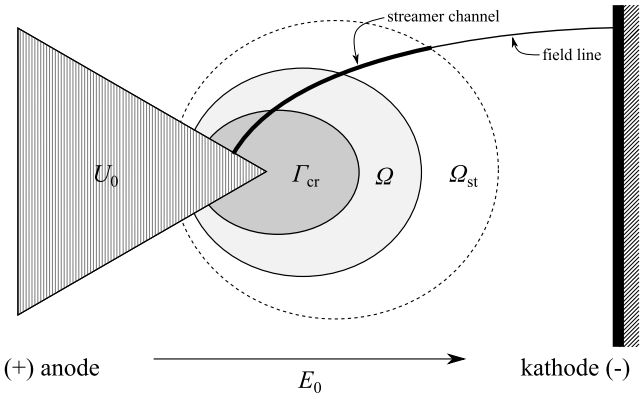

FIGURE 7. Schematic illustration of the different areas which are relevant for streamer development. Adapted from [71].

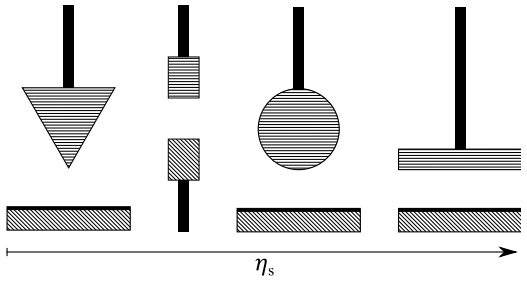

FIGURE 8. Examples of discrete arrangements with different degrees of uniformity η_s in HV technology. Adapted from [19].

HV experiments that stable PDs can occur under a degree of uniformity (Schwaiger's utilization factor) of $\eta_s < 0.2$ (strongly nonuniform) [72]. In the streamer mechanism, it is important whether the tip is positive or negative since the ignition voltages ($U_{i+} < U_{i-}$) and the PDIV differ due to the different space charge distribution (polarity effect) [19], [20]. Note that these are in any case metallic electrodes and that when the insulation system of LV machines is imitated in the form of enameled wire pairs, it is a matter of dielectric barrier discharges (DBD) [73]. In addition to field distortion caused by streamers, space charges of the same polarity (homocharges) can form in front of the electrodes at high field strengths, which also influence the field characteristics (see Fig. 9a). As the space charge increases, the field strength can even decrease to the stage where PDs extinct and then ignite again after the space charges have recombined or drifted away. This results in a regular intermittent sequence of pulses, the so-called Trichel pulses [74]. Space charges of opposite polarity (heterocharges) arise from charge drift and produce field strength enhancement in front of the electrodes (see Fig. 9b). In this context, polarity changes at bipolar voltage are of importance. In the context of space charges, there are some investigations on wire pairs [4], [75], [76], [77], [78].

E. DYNAMIC DESCRIPTION OF GAS DISCHARGES

For the previously described discharge mechanisms, stationary conditions were assumed. However, if fast-rising

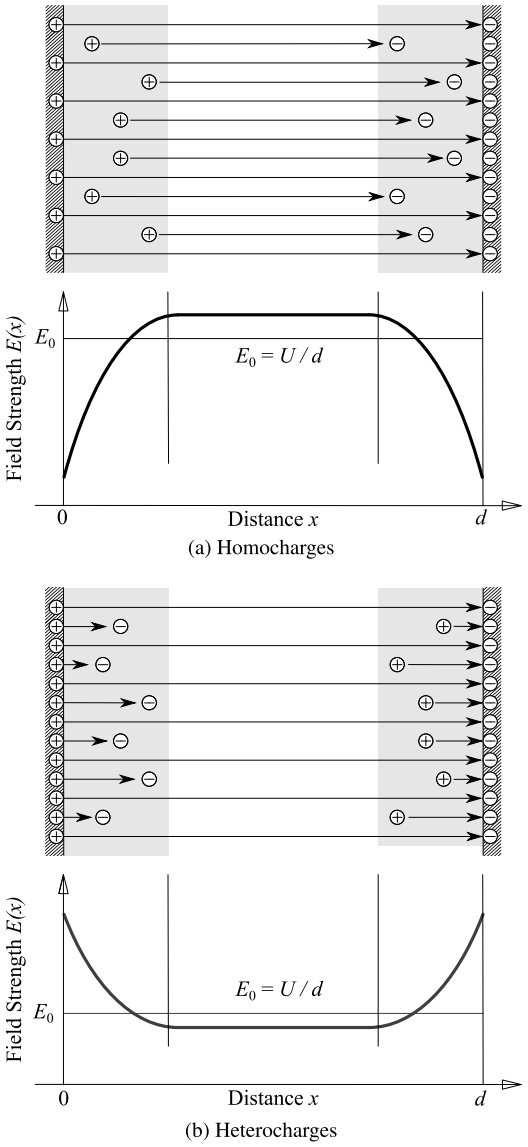

FIGURE 9. Schematic illustration of homocharges and heterocharges with their associated field characteristics. Adapted from [19].

voltage stresses are present, the discharge mechanisms must also be considered under the aspect of statistical time effects. These have long been established in high voltage technology [19], [20].

When the static breakdown voltage U_0 is exceeded, at which a discharge would be possible in the steady-state case, a statistical time lag t_s passes first, after which a start electron is available. If a conductive channel develops within the streamer formation time t_f, the voltage collapses in the spark time t_c as a result of the breakdown which occurs in the case of a uniform field distribution. In sum, this results in the delay time t_D.

$$t_D = t_0 + t_s + t_f + t_c \tag{9}$$

The time t_0 until the static breakdown voltage is reached is reduced by a high dv/dt. For illustrative purposes, Fig. 10a

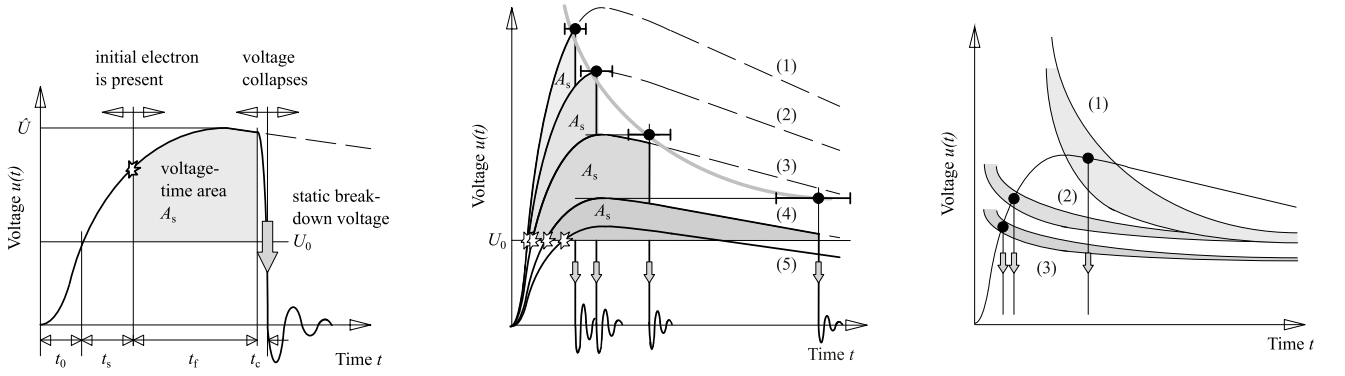

(a) Breakdown/discharge delay t_D and the specified voltage-time area A_s according to (10)

(b) Determination of a voltage-time characteristic curve according to (10)

(c) Different voltage-time characteristic curves: (1) strongly nonuniform field distribution, (2) uniform field distribution, (3) constructively desired flat curve (lightning arrestor)

FIGURE 10. **Dynamic character of gas discharges. Adapted from [19].**

does not show any overshooting, as occurs at the motor terminals. Due to the volume effect (see Section IV-E2), the ignition delay time t_s decreases with an increase of the stressed gas volume. This relationship is also known as the volume-time theory [19] and is considered in some papers for calculating the PDIV [45], [77], [79]. In cavities in solid dielectrics (see Section III-F), the ignition delay time t_s and for nonuniform fields, the formative time lag t_f can reach very large values [19]. For pulsed voltages, the channel mechanism can be assumed in practice [19]. The more the electric field strength exceeds the reference field strength $E_0 = U_0/d$, above which a streamer can develop, the higher the streamer propagation velocity of the streamer. Hence, increasing the DC link voltage would lead to a higher streamer propagation velocity, whereas fast switching would allow a higher field strength if only the time dynamics are considered. The voltage-time area A_s plotted in Fig. 10a is a constant quantity for a specified insulation arrangement, which strongly depends on the exact voltage form and the degree of uniformity of the arrangement and is described by Kind's equal voltage-time area criterion [19], [80]:

$$\int_{t_0+t_s}^{t_0+t_s+t_f} \{u(t) - U_0\}\,\mathrm{dt} = A_s = \text{const} \tag{10}$$

Despite exceeding the static breakdown voltage U_0, if the necessary voltage-time area A_s (curve 5 in Fig. 10b) is not reached, the streamer growth will stop and no breakdown or in the case of nonuniform field conditions, no PD will occur. For different rise times, the relation of the peak value to the time, at which breakdown occurs, results in a characteristic curve [19], [29]. The breakdown voltage increases from long rise times to short rise times, as can be seen in Fig. 10b.

In Fig. 10c, principal voltage-time characteristic curves for different degrees of uniform electrical field distribution are shown. In the case of strong nonuniformity, a larger breakdown and/or discharge delay occurs because the highly stressed gas volume is comparatively small and the streamer propagation velocity v_{st} is much lower in the low-field region. As a consequence, the voltage-time area is larger for nonuniform field distributions. However, with increasing nonuniformity, the PDIV also decreases.

F. DISCHARGES IN SOLID AND MULTILAYER DIELECTRICS

The discharge process that occurs in insulation paths with solid dielectric is called electrical treeing (see Fig. 11) [81], [82], [83]. In the case of technical insulators, inhomogeneities are present in the solid dielectric in a microscopic form in the lattice structure of the solid as a result of amorphous areas and in a macroscopic form from defects (cavities, cracks, etc.) or at transitions between two materials. This results in nonuniform stress on the insulating path, which can be amplified by the geometry of the arrangement (e.g., sharp edges). These inhomogeneities are stressed by the electric field until discharges occur [60]. In the case of gas-filled voids, the discharge mechanism can be characterized by the physical descriptions of gas discharges. Furthermore, a not insignificant number of publications deal with the influences of the cavity geometry concerning PD behavior [60].

In the areas of the solid dielectric, the energy-band model of solid-state physics is approached. The conduction band is found to have very few free electrons. Electrons can be released from the metallic electrodes by external field emission as in gas discharge. In the case of internal field emission, electrons are raised from the valence band into the conduction band by the influence of the electric field, which then contribute to charge transport. In an ideal crystal structure, extremely high field strengths would be necessary for this. The irregularities in technical insulators create additional states between the conduction and valence bands – the traps. These can be either unoccupied or occupied by electrons (donor). Starting from the traps, the electrons are raised

FIGURE 11. Typical propagation of an electrical tree which has incepted at a tip. From [84].

into the conduction band under the influence of the electric field and can then settle again in other traps. The process is called "hopping" [19], [81], [85]. In solid dielectrics, as in gaseous dielectrics, space charges can also form in front of the electrodes depending on the level of the field strength. Surface charges can furthermore form at boundary layers. Due to the erosion process of the internal PDs, which successively enlarge the cavities, tree-like structures are formed, which grow along the field path and finally lead to erosion breakdown (see Section IV-A).

In the case of an internal PD, the field distribution in the surrounding area of the defect also changes and charge displacements occur in the defect as well as at the electrodes [19]. To describe the internal PDs, a capacitive equivalent circuit is assumed for AC voltage (see Fig. 12a) [86], [87]. Here, C_c is the cavity capacitance, C_s is the partial capacitance in series with the cavity, and the parallel capacitance C_I is approximately the capacitance of the entire insulation arrangement. When the ignition/inception voltage U_i is exceeded for the first time, the voltage collapses until the PD, which is modeled by discharging the cavity capacitance, extincts again (U_e). Thereafter, the voltage $\Delta U = U_i - U_e$ recharges the cavity capacitance by capacitive displacement current until the next PD starts. The voltage at the cavity corresponds to the voltage, which would result across C_c by the voltage divider of C_s and C_c (see $u_{c,vd}(t)$ in Fig. 12b), but repetitively shifted by ΔU in the ordinate direction. In this equivalent circuit, the phase shift is neglected, but it is present in practical applications when a conductive layer is formed by the decomposition products produced when the polymer chains break up in the cavity [19], [60]. The PD extinction voltage (PDEV) can be significantly lower than the PDIV due to the shift in the negative ordinate direction by ΔU,

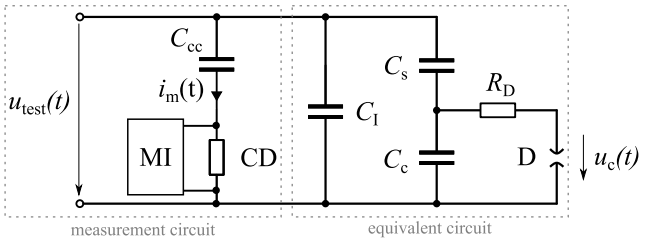

(a) Equivalent circuit for internal PD at gas-filled defects. Label: $u_{test}(t) = \hat{u} \cdot \sin(\omega t)$ = test voltage, C_{cc} = coupling capacitor, $i_m(t)$ = measured current, MI = measurement instrument, CD = coupling device, C_I = insulation capacitance, C_s = serial capacitance, C_c = cavity capacitance, R_D = discharge resistance, D = discharge path, $u_c(t)$ = cavity voltage. Adapted from [19], [86]

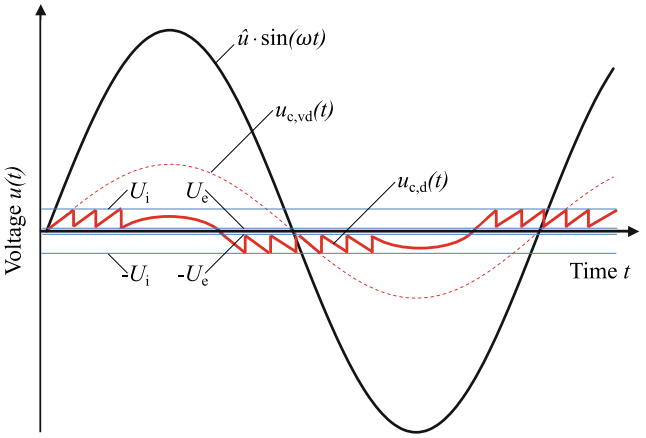

(b) Voltage curve of the equivalent circuit of the cavity at AC. Label: $u_{test}(t) = \hat{u} \cdot \sin(\omega t)$ = AC voltage, $u_c(t) = u_{c,vd}(t)$ = theoretical voltage drop across C_c without discharge (voltage divider), $u_c(t) = u_{c,d}(t)$ = voltage drop across C_c with discharge, U_i = (partial) discharge inception voltage, U_e = (partial) discharge extinction voltage. Adapted from [19], [86]

FIGURE 12. Equivalent circuit and the corresponding voltage curve for internal PD.

because PDs continue to occur despite the lowering of the AC voltage. This behavior plays a role, among others, in the classical interpretation of PD measurements (see Section IV-E). The simple equivalent circuit is not considered suitable by some authors and a model is proposed in which PDs are represented by dipoles [86], [88].

If no defect initiated the process of electrical treeing, it is considered an initial breakup, in which a local overstress of the insulation path takes place due to charge carrier injection [60]. In addition to the erosion breakdown that results, a thermal breakdown can occur in solid dielectrics due to thermal overstress (see Section IV-A). When discrete insulation paths of electrical machines are examined, multilayered dielectrics occur in them. Due to tangential field stress, surface discharges can occur in the gas layer/volume at comparatively low potential differences.

IV. AGING, LIFETIME MODELS, AND TESTING

A. DEGRADATION IN THE INSULATION SYSTEM

Over their lifetime, electric motors are subjected to several stresses during operation. Continuous or intermittent

exposure to stress irreversibly changes the physical and chemical properties of the insulation system negatively. The process of changing – the aging process – is based on aging mechanisms, which can be intrinsic or extrinsic [84]. Intrinsic in this context means that (slow) aging occurs in the absence of defects in the insulation system. Extrinsic means that (faster) aging occurs in the presence of unintended defects [84]. The stresses and mechanisms are divided into four classes, the so-called TEAM factors (thermal, electrical, mechanical, ambient), which interact directly or indirectly [84]. The study of the damaging effects on the insulation system is the subject of current research, in which mostly one or two TEAM factors are focused, even if in real operation all aging factors are always simultaneously present in different levels of severity due to their coupling and feedback. The synergistic effects could be positive as well as negative. In this paper, as already mentioned in the introduction, the focus is limited to the electrical influencing factors. The following subsections IV-A1 to IV-A3 refer to Fig. 13.

1) THERMAL BREAKDOWN

The electrical potential difference between the conductive components of the electrical machine determines the electrical stress on the insulation system. This results in frequency- , temperature- , and field strength-dependent dielectric losses. Together with the load-dependent ohmic losses caused by the machine phase currents, those dielectric losses are mainly responsible for the electrically induced heating of the insulation system. As a result of the increase in conductivity, the dielectric losses P_δ follow an exponential curve [19]:

$$P_\delta = U^2 \cdot \omega \cdot C \cdot \tan(\delta_a) \cdot e^{\beta(T-T_a)} \tag{11}$$

With δ_a the loss angle at ambient temperature T_a and β being a material-specific temperature coefficient. If the thermal power added exceeds the thermal power dissipated over a certain time, this results in a thermal breakdown in the solid dielectric. In this context, the term ''thermal breakdown voltage'' is used instead of ''breakdown field strength''. In addition, heat accelerates further electrical damage processes through chemical degeneration processes at the atomic scale [19].

2) EROSION BREAKDOWN

Organic insulating materials (type I [27]) are successively degraded by the erosion effect of PDs at repetitive impulse and sinusoidal alternating voltages until erosion breakdown occurs.

PDs can occur with uniform field distribution in inhomogeneous dielectrics. Inhomogeneities can be attributed to many causes. On the one hand, a poor manufacturing process can cause defects, such as air-filled cavities or particle-contaminated inclusions. Defects can also develop over time in the form of delamination and cracking. On the other hand, abrupt changes in permittivity, density, or anisotropy of the dielectric are associated as material-related inhomogeneities and usually cannot be completely excluded during manufacturing. The result are PDs that stress the inhomogeneous spot until a field strength change occurs. The faults increase in size like a tree (electrical treeing) and finally lead to an erosion breakdown (green line path in Fig. 13).

If a (nearly) homogeneous defect-free dielectric is present, then initial breakup can occur as a result of a nonuniform field distribution and the local overstressing of the dielectric associated with it (red line path in Fig. 13) [60]. In the case of nonuniform field distribution in the gaseous dielectric, external PDs (corona) occur which, after sustained exposure, lead to erosion breakdown, just as in the case of surface discharges at interfaces between solid and gaseous dielectric.

3) ELECTRICAL BREAKDOWN

If the field distribution in the gaseous dielectric is uniform or slightly nonuniform ($\eta = 0.8 - 1$), no PDs occur. When the arrangement-specific critical field strength is exceeded, breakdown immediately follows (blue line path in Fig. 13). In contrast, in the case of a nonuniform field distribution, a stable glow phenomenon occurs due to the shielding effect of the space charge at the corona inception voltage (U_i), which is far below the breakdown voltage (U_B). The electrical breakdown is usually associated with the system failure of the electrical device.

4) PDs AS AN AGING FACTOR – THE SOURCES IN ROTATING ELECTRICAL MACHINES

In round wire windings, the worst and not unusual case is when the first and the last turn of a coil are directly adjacent to each other. Inverter feed with fast switching transients results in a highly nonlinear transient voltage distribution along the winding, which causes up to 90% of the total phase-to-ground voltage to drop over the first turn at a switching event [3], [27]. Consensus in literature is this is the weakest point of the insulation system in LV machines, and thus determines the electrical resilience of the machine. A simple imitation of the winding insulation are wire pairs. Therefore, most publications deal with the study of the insulation issue on wire pairs [3], [44], [45], [46], [49], [68], [77], [79], [89]. In contrast, there are very few contributions dealing with flat wire/hairpin windings [90], [91], [92], [93], [94]. In addition, the entire insulation difficulty is extremely parameter sensitive in all domains, including the decisive electrostatic field distribution resulting from the geometry, as exemplified in Fig. 14. As a consequence, the results from the investigation on round wire windings are not comparable to those of hairpin windings and a considerable research effort and experimental validation of the latter is still required. The winding type, the machine geometry, the (transient/stationary) voltage distribution, and the structure of the insulation system result in different locations where PDs develop, which are associated with unequal probabilities of occurrence and damage risks. Considering round wires, PDs must not only evolve at the before discussed weakest point – the winding insulation – but can also occur between the conductor and the laminated

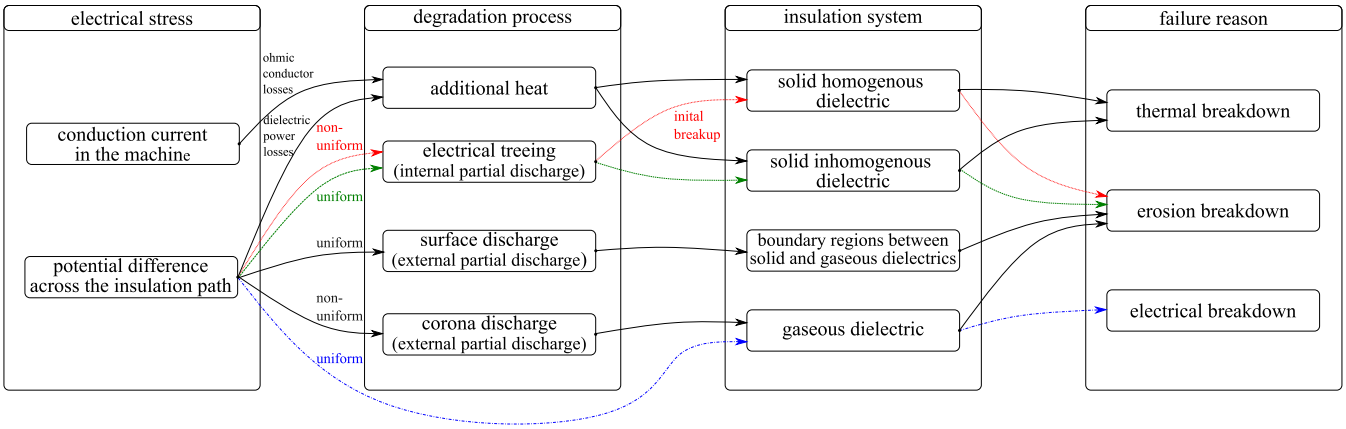

FIGURE 13. Sequential illustration of the possible degradation processes in the insulation system of the machine.

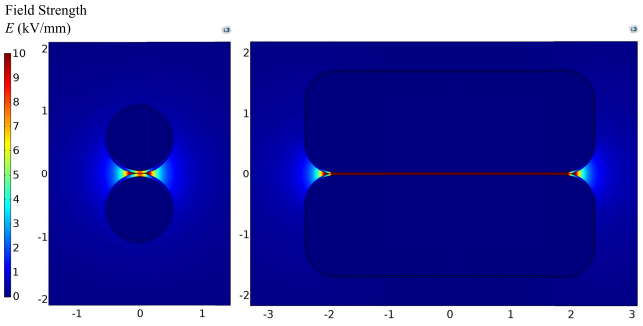

FIGURE 14. Electrical field distribution. Implemented in COMSOL Multiphysics® 5.6 with conductor diameter of $r_c = 1$ mm and realistic dimensions of a hairpin, insulation thickness $d_i = 50$ µm, voltage between the conductors $U = 800$ V. The scaling of the axes is in (mm).

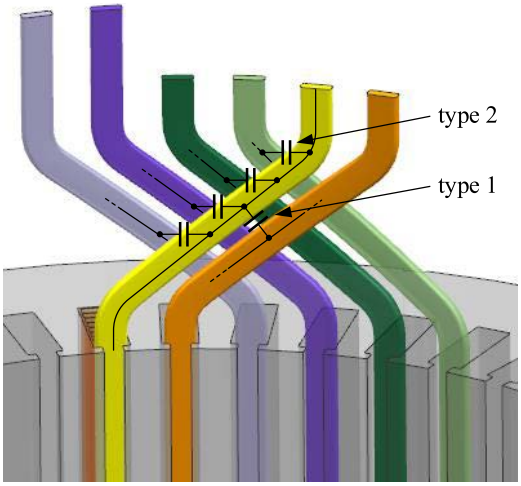

FIGURE 15. Section of the CAD model of our exemplary investigated machine. Label: type 1 insulation path between two conductors origin from parallel phase branches, type 2 phase-to-phase insulation path where PD occurs most frequently.

core with earth potential separated by the slot liners [56]. This is also possible with flat wire windings in contrast to the worst-case scenario with round wire windings, which does not occur in the slot due to the defined winding geometry. PDs and surface discharges can also occur in the winding head. Geometrically, all insulation paths of a machine (phase-to-phase, phase-to-ground, turn-to-turn) meet in this area. PDs between turns can be geometrically avoided in the flat wire winding in the winding head, depending on the winding design.

The impregnation resin and the insulation paper increase the electrical resilience compared to the enamel insulation. However, defective impregnation, where delamination, cracks, and other air-filled inclusions are present, reduces the electrical resilience of the insulation system, because in the voids an enhanced field strength compared to the background field leads to erosive PDs. HV machines differ from LV machines by their field control – the corona protection – as already mentioned in Section II-A, which LV machines do not have. In the exemplary machine, we considered, it has been shown that the insulation problems occur mainly between two phases in the winding head (see type 2 in Fig. 15), which has not yet been addressed in any paper presently published. This is where the highest voltage stress in terms of magnitude is present in the machine.

B. ACCELERATED AGING AND AGING INDICATORS

In general, the lifetime of an electrical insulation system is equivalent to the time difference until an electrical breakdown occurs. For the design of (electrical) systems in the meaning of production goods, accelerated life tests (ALT) are used in the manufacturing industry to acquire data from which statements on the reliability and quality of a product over its operating time are to be derived within an economically justifiable framework. The acceleration of aging is achieved by subjecting the complete system, a subsystem, an individual component, or an imitation thereof to higher stress (see the solid gray line in Fig. 16) than can be expected during normal operation (see the dashed gray line in Fig. 16) in the life of the product later on [33], [95]. In addition to a lifetime prediction based on statistical methods, possible sources of error and weak points in the design can also be identified.

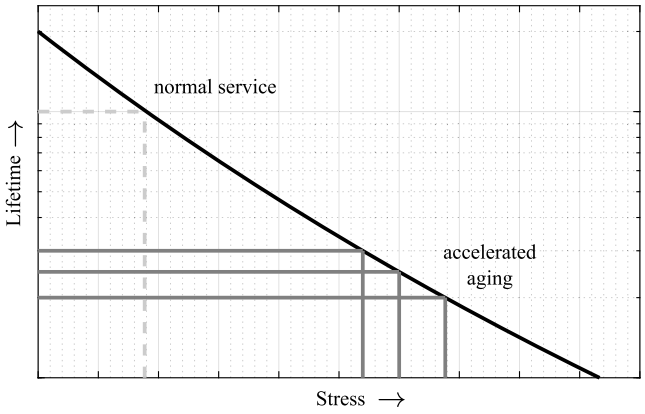

FIGURE 16. Principle of accelerated aging tests in a typical semi-logarithmic lifetime-stress diagram. Adapted from [101].

A differentiation is made between single-factor aging and multi-factor aging [96], [97]. The following factors are mentioned in literature with which acceleration can be achieved regarding electrical aging:

- increase of the voltage level
- increase of the switching slew rate ($\mathrm{d}v/\mathrm{d}t$)
- increase of the switching frequency

In addition to increasing the stress level, the aging rate can be enhanced by environmental factors such as heat and humidity. This causes the chemical reaction processes and physical processes of the aging mechanisms to take place more quickly. In literature, a large number of publications can be found where solely electrical aging or solely thermal aging is considered and the effects of the electrical acceleration parameters are investigated (single-factor aging). Furthermore, in addition to the number of aging factors, the type of stress must be distinguished: constant, cyclic, incremental, or transient. As an example, constant voltage and voltage-rise tests with DC can be mentioned here. Multi-factor aging is usually performed with electrical and temperature acceleration. Thermal cycling is also studied as thermo-mechanical aging [96]. Another focus is on the influence of pressure on the discharge behavior, as this is important for the electrification of aircraft [43], [98], [99], [100]. In the context of aging experiments, six subdisciplines emerge, each of which has problems of a practical and theoretical/statistical nature and, partially, a feedback character to each other:

1) analysis and definition of the problem
2) analysis and modeling of the system to be investigated
3) planning of the experiments and construction of the test bench
4) execution of the experiments and data acquisition
5) data evaluation and interpretation
6) derivation of lifetime models and calculation of reliability metrics

This and the following sections are intended to address only the main basic ideas of accelerated aging tests and to provide an overview of the lifetime models as well as refer to the standard. Therefore, not all listed points will be dealt with in their entirety. One of the problems of electrical aging is the existence of certain threshold values above which the aging mechanism may change at momentary stress. However, these thresholds are difficult to determine in practice without in-depth knowledge of the mechanism. In addition, the aging mechanism may change over time due to the continuing aging progress.

Another major problem derived from the principle of accelerated aging is the implication of acceleration. There is currently no consensus in literature on a suitable aging indicator. This conclusion can be drawn from Table 2, which results from a broad literature evaluation.

Table 2 is divided vertically into continuous (top) and discrete (bottom) influencing factors, which are separated by the double line. In addition to electrical aging, thermal aging is also included in the influencing factors, since this is often considered in the framework of electrical stress. The duty cycle was not part of the enumeration of relevant continuous acceleration factors before, because there were fewer publications found dealing with its variation and impact. The arrows for the continuous factors indicate an increase (↑), decrease (↓), or no discernible trend or influence of the aging indicator (↔). For the discrete factors of voltage shape (sinusoidal or pulsed) and polarity (unipolar and bipolar), only a discrete distinction between no influence (↔) and influence (↕) is made.

For thermal aging, all publications agree that the PDIV and insulation resistance (IR) decrease and $\tan(\delta)$ increases during aging. For capacitance, the sources given are contradictory. For the PDEV, only one contribution was found in the context of thermal aging.

Regarding the electrical aging of LV machines, the PDIV is the most frequently studied indicator. RPDIV stands for repetitive PDIV and is used exclusively for pulsed voltages. Concerning the aging factor of the switching frequency, Table 2 shows that on the one hand the sources contradict each other and most publications attest no influence.

When increasing the DC link voltage, the PDIV is not listed since a voltage increase is inherent in a PDIV measurement. However, the magnitude and number of PDs and the PD probability (not listed in the Table 2) are related to aging. For the PD magnitude, which is a related parameter of the specific measurement setup used (see Section IV-E), a tendency to increase is identified; for the number of PDs, there is no general agreement on the influence.

In the case of the duty cycle and the switching slew rate or the rise time, there is also no clear picture for the PDIV and PD magnitude. For the PDEV, only one source was found that investigated the influence of the $\mathrm{d}v/\mathrm{d}t$.

Concerning the comparability between sinusoidal and pulse as well as unipolar and bipolar voltage or its influence, opposite results were found in the publications. Thereby, the result varies between impulse voltages are more damaging, equivalent, less damaging or differences exist but do not show

TABLE 2. Correlation between investigated aging factors and aging indicators.

category	aging factor	gradient	aging indicator	gradient	reference
electrical	switching frequency	↑	PDIV	↑ ↔	[102] [43], [46], [76], [103], [49], [104]
			RPDIV	↓	[77], [105]
			PDEV	↓	[46]
			PD magnitude	↑ ↔ ↓	[76] [73], [103] [77], [106], [107]
	voltage level	↑	PD magnitude	↑	[6], [108]
			PD number (m)	↑ ↔	[108] [73]
	duty cycle	↑	PDIV	↑ ↔ ↓	[35] [103] [102]
			RPDIV	↓	[109]
			PD magnitude	↑ ↓	[107], [110] [103]
	$\mathrm{d}v/\mathrm{d}t$	↑	PDIV	↑ ↔ ↓	[35], [62], [77], [103], [107] [43], [49], [102] [79]
			PDEV	↓	[111]
			PD magnitude	↑ ↔	[77], [107], [112] [103]
thermal	temperature	↑	PDIV	↓	[46], [77], [106], [113]–[116]
			PDEV	↓	[46]
			capacity	↑ ↓	[117], [118] [77], [119]–[121]
			$\tan(\delta)$	↑	[117], [121]
			IR	↓	[89], [119]–[122]
electrical	voltage type		PDIV	↕ ↔	[2], [60], [68], [108], [112], [113], [123]–[125] [43], [76]
	polarity			↕ ↔	[35], [76], [108], [109] [4], [43], [49]

arrow meanings: ↑: positive change, ↔: no change, ↓: negative change, ↕: positive or negative change

a clear trend compared to a sinusoidal voltage. The same applies to the influence of polarity.

In addition, some authors found an interaction between the named aging factors. The type and extent of these reported influences as well as their interpretation vary among the authors. As a result, this aspect is not further discussed here. In summary, it can be stated that, despite a large number of publications, there is more dissent than consent about the influencing factors and their impact on measurable aging indicators. Finally, this is because the measurement methods are also fraught with difficulties and the measurement setups and conditions differ considerably in some cases.

C. LIFETIME ESTIMATION

The models for a lifetime estimation are either based on physical descriptions (section IV-C1) or a statistical approach is adapted with empirically acquired data and cumulated experience (section IV-C2). A combination of both is also possible [96].

1) PHYSICAL MODELS FOR ELECTRICAL AGING

A physical model developed by Crine describes the process of aging in solid polymer insulating materials based on electrically induced mechanical deformation of intermolecular Van der Waals bonds, which result in submicrocavities where electrons can be injected [126]. Above a critical field strength, the necessary activation energy ΔG is exceeded, the free path length of the electrons reaches a constant maximum value and the polymer chains are broken. This damage mechanism leads to electrical breakdown after a certain time [126], [127], [128].

$$L \simeq t \simeq \frac{h}{2k_\mathrm{B}T} \cdot \exp\left(\frac{\Delta G}{k_\mathrm{B}T}\right) \cdot \operatorname{csch}\left(\frac{e\lambda E}{k_\mathrm{B}T}\right) \tag{12}$$

L stands for the lifetime, t for the time until the state of bond disruption starts, h for the Planck constant, k_B for the Boltzmann constant, T for the temperature (in K), csch for the hyperbolic cosecant, ΔG for the activation energy, λ for the free path length, E for the electrical field strength and e for the charge of an electron. At high field strengths, the equation reduces to an exponential relationship:

$$L \simeq t \simeq \frac{h}{2k_B T} \cdot \exp\left(\frac{\Delta G - e\lambda E}{k_B T}\right) \tag{13}$$

2) EMPIRICAL MODELS FOR ELECTRICAL AGING

The literature contains a large number of publications on the Inverse Power Law, which follows a heuristic approach to electrical aging by PDs and describes the average expected lifetime as a function of the electric field strength E [97], [129]. The law is also used for applications other than electrical aging and is recommended in the standard IEC 60505 [84].

$$L = 1 - a_1 \cdot E^{b_1} = a_1 \cdot E^{-b_1} \tag{14}$$

In addition to the Inverse Power Law, the Exponential Law is also commonly used [129]. a_1, a_2, b_1, and b_2 are constants to be determined via experiments.

$$L = a_2 \cdot e^{-b_2 E} \tag{15}$$

Other models exist, but they have not gained as much popularity and likewise show an exponential (different) characteristic [34], [96], [129], [130].

3) MODELS FOR THERMAL AGING

Since heat is a secondary effect of electrical stress, the quantitative relationship will be briefly described here. With the Arrhenius equation, the reaction rate r or the lifetime is described with the temperature via an exponential relation [131]. The physical mechanism underlying is an increase in the mobility of the charge carriers and an increase in the occupancy of the conduction level (according to the energy-band model) as a result of the energy supply (activation energy E_a) in the form of heat. The consequence is an exponential increase in conductivity, which is associated with an increase in dielectric losses.

$$L \simeq \frac{1}{r} = A_1 \cdot \exp\left(\frac{E_a}{k_B T}\right) \tag{16}$$

With k_B the Boltzmann constant, T the temperature, and A_1 being a system-specific coefficient. Dakin modified the equation for electrical insulation systems based on Arrhenius' findings [132]. Here, A_2 and B_2 are system-specific constants to be determined empirically.

$$L = A_2 \cdot \exp\left(\frac{B_2}{T}\right) \tag{17}$$

A common feature of the empirically found laws in the form of mathematical expressions is that they contain arrangement-specific model variables that can only be determined by testing and cannot be transferred to other arrangements. This underlines the parameter sensitivity and specificity of the insulation topic.

4) STATISTICS OF LIFETIME ESTIMATION

The statistical method of regression analysis is used to predict or estimate aging indicators from which the lifetime can be derived or the lifetime itself is predicted. The generation of a lifetime curve has four degrees of freedom:

1) choice of the lifetime model
2) choice of the regression curve
3) choice of the estimation method of the regression parameters
4) choice of the distribution function

The lifetime models have already been presented. The regressions for curve fitting to the measured values can have these four forms: linear (18), exponential (19), logarithmic (20), and power series (21). The parameters α and β are determined by the estimation method of the regression analysis.

$$y(t) = n + m \cdot t \tag{18}$$
$$y(t) = n \cdot e^{mt} \tag{19}$$
$$y(t) = n + m \cdot \ln(t) \tag{20}$$
$$y(t) = n \cdot t^m \tag{21}$$

In the standard 60172 [133] the Arrhenius equation and linear regression are used. Besides the conventional curve fitting ((18) - (21)), in [89] a neural network was trained with the Bayesian regularization backpropagation (BRP) algorithm. Good results were obtained, so modern methods can also be applied. The least squares method (LS) is commonly used to minimize the residuals. Other common methods are the least absolute residual (LAR) method, which minimizes the signed residuals instead of the residual sums of squares, and the bisquare method, which weights the residual sums of squares [101].

Since the variables relevant to lifetime, such as the PDIV, are statistical random variables, a theoretical distribution function must be assumed for the measured values. In small test batches, the two-parameter Weibull distribution has been found to be the most suitable distribution [19], [49], [81]. The failure probability $F(t)$ depends on the scale parameter α and the shape parameter β (see Fig. 17).

$$F(t) = 1 - \exp\left(-\left(\frac{t}{\alpha}\right)^{\beta}\right) \tag{22}$$

To account for the strong dispersion, confidence intervals are stated in publications, which depend on the predefined statistical certainty (the confidence level), the number of samples, and the distribution or the spread [135], [136]. The confidence level in literature is usually set very conservatively at 90% (two-sided bounds) [49]. The following methods exist for calculating the intervals, the first mentioned being the most commonly used [34], [49]:

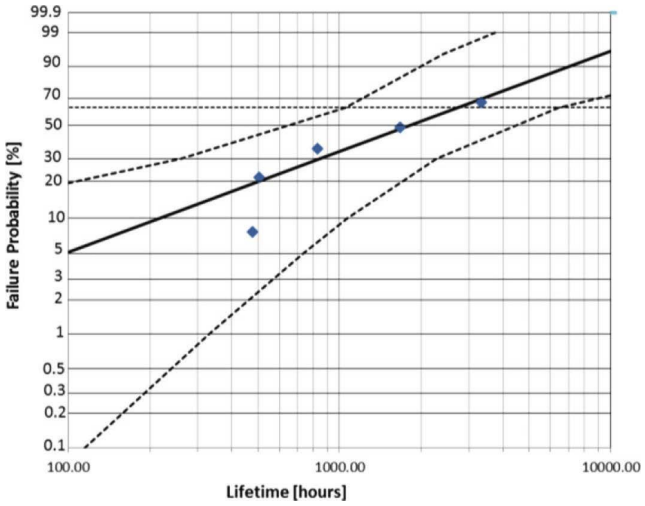

FIGURE 17. Typical Weibull plot with two sided confidence bounds (dotted lines) [134].

- Monte Carlo pivotal bounds
- likelihood ratio bounds
- beta-binomial bounds
- Fisher's matrix bounds

D. RELEVANT STANDARDS

The relevant standards are to be discussed here since a large number of publications refer to standards and some papers also discuss them with regard to their suitability for WBG devices [43], [46], [77], [93], [116], [123], [137].

The standard 60034-18-41 [27] is intended for type I (< 700 V) PD-free machines and standard 60034-18-42 [138] is intended for type II (> 700 V) PD-resistant machines, as in Section II-A mentioned. The standard for PD-resistant machines is completely different in its test procedure from the test procedures for PD-free machines. The purpose of the standard for type I machines is to qualify PD absence by performing tests. The first stage of the test in the form of a cyclic sequence to be run through is the qualification test, in which wire pairs or motorettes/formettes are subjected to thermal aging cycles and further conditioning (mechanical and environmental stress). It is important to note that electrical aging is not part of the test procedure, as significant electrical aging is only assumed in the presence of PDs. The second stage is the type test, in which complete windings or the machine to be qualified are used as test specimens. The tests are considered to have been passed if it has been demonstrated by a series of tests that the (R)PDIV is above a specific voltage limit. The calculation of this limit is part of the standard and depends on the stress level of the respective application.

1) CALCULATION OF THE TEST VOLTAGE ACCORDING TO THE STANDARD

To perform the qualification test, the electrical stress that the machine is likely to experience during operation must be determined. To this end, the standard claims that the peak-to-peak voltage $\hat{U}_{pk-pk}$ is "the" decisive variable in electrical stress due to the space and surface charges that occur. Furthermore, it is concluded that a unipolar voltage should produce the same stress as a bipolar voltage with the same peak-to-peak value. Hence a factor of 2 is motivated in the following equation, which is valid for a two-level converter:

$$\hat{U}_{\mathrm{ph-ph}} = 2 \cdot \mathrm{OF} \cdot (U_{\mathrm{DC}} + \Delta U_{\mathrm{DC}}) \tag{23}$$

With OF the overshoot factor, which expresses the ratio of the peak voltage to the steady-state DC link voltage U_{DC}, and ΔU_{DC} being the DC link voltage fluctuations. A factor of $\frac{\sqrt{2}}{2}$ is assumed for the phase-to-ground voltage, which depends on the grounding system and is due to the possible potential difference between ground potential and DC zero potential:

$$\hat{U}_{\mathrm{ph-grd}} = \frac{\sqrt{2}}{2} \cdot \hat{U}_{\mathrm{ph-ph}} \tag{24}$$

And finally, the winding/turn-to-turn voltage $U_{\mathrm{t-t}}$ depends on the rise time factor $a(t_{\mathrm{r}})$ and can be taken from a diagram in the standard, which is related to the jump voltage U_{j} $\left(= U_{\mathrm{ph-grd}}\right)$ at the motor terminals. In the standard, a rise time of 0.3 µs is used as default:

$$\hat{U}_{\mathrm{t-t}} = a(t_{\mathrm{r}} = 0.3\,\mu\mathrm{s}) \cdot U_{\mathrm{j}} = 0.7 \cdot \hat{U}_{\mathrm{ph-grd}} \tag{25}$$

Assuming a DC link voltage U_{DC} that is switched from 0 V to 800 V and stresses the insulation system with a magnitude of 800 V during the switched state should produce the same stress as a bipolar voltage that is switched from -400 V to 400 V and stresses the insulation system with a magnitude of 400 V during the steady state. If (1) from Section II is applied, it results in half the field strength in magnitude for the same insulation arrangement. This implies that a space-charge generated Poisson field superimposed on the Laplace field would have to produce a field strength that would cause equivalent stress.

Apart from the consideration of "the" decisive stress parameter $\left(\hat{U}_{pk-pk}\right)$, additional factors are introduced in the standard to further quantify the stress. As already mentioned, fast switching causes voltage overshooting, which is to be taken into account by four stress categories that are dependent on the pulse rise time. For minor overshoot, stress category A (benign) would be selected and the overshoot factor is 1.1. For inverter-fed machines where the stress is not known more precisely, category C (severe) is recommended, where OF is in the range of 1.5 to 2.0 times the steady-state voltage.

For sinusoidal voltages, as described in Section III-F, a hysteresis effect on the PD behavior in the form of a reduced PDEV has been observed, which is taken into account here with a factor of 1.25. According to the standard, the increase in winding temperature from 25 ° C to 155 ° C led to a reduction in PDIV of 30%, hence the factor here is 1.3. Due to the cooling effect of the adjacent windings in a slot,

TABLE 3. Calculation of the test voltage according to IEC 60034-18-41 [27]. The rightmost column is the maximum of the product of all factors and constitutes the test voltage.

test type	insulation path	permitted test specimens	PDIV enhancement factors			$\hat{U}_{\mathrm{pk-pk}}$ enhancement factors		test voltage U_{test} at stress category C
			PD hysteresis	temperature	aging	U_{DC} fluctuations	OF	
qualification test	phase-to-phase	M/F, CW	1.25	$1.00-1.30$	1.00	1.10	$1.10-2.00$	$7.15 \cdot U_{\mathrm{DC}}$
	phase-to-ground	M/F, CW		$1.00-1.10$				$4.24 \cdot U_{\mathrm{DC}}$
	turn-to-turn	TP, M/F, CW		$1.00-1.30$				$3.51 \cdot U_{\mathrm{DC}}$
type test	phase-to-phase	CW	1.25	$1.00-1.30$	$1.00-1.20$	1.10	$1.10-2.00$	$8.58 \cdot U_{\mathrm{DC}}$
	phase-to-ground			$1.00-1.10$				$5.08 \cdot U_{\mathrm{DC}}$
	turn-to-turn			$1.00-1.30$				$4.20 \cdot U_{\mathrm{DC}}$

TP = twisted pair, M/F = motorette/formette, CW = complete winding

a reduced value of 1.1 is assumed for the phase-to-ground test. The factors for temperature and PD hysteresis were investigated in [46] and it is concluded by the author that they are not suitable due to their dependence on temperature, switching frequency, and voltage form. In the case of the qualification test, aging is the object of investigation, so here the factor is set to 1, unlike in the type test, where the influence is taken into account with a factor of 1.2. Due to voltage fluctuations in the DC link ΔU_{DC}, another factor of 1.1 is introduced for a fluctuation of 10%. Other factors, such as humidity or pressure, which can have a considerable influence on PDIV, are not taken into account in the standard. The maximum of the product of all factors, which is equal to the test voltage, can be seen in the rightmost column of Table 3.

At this point, it should be emphasized that the safety factors are not subject to sufficiently substantiated evidence and therefore the application of the factors should at least be questioned. Moreover, the statement in the standard that sinusoidal and impulsive stresses produce equivalent results may be strongly doubted, as has been done in some publications [43], [62], [123].

2) THE PROCEDURE OF THE QUALIFICATION TEST FOR PD-FREE MACHINES (TYPE I)

The test procedure in the standard IEC 60034-18-41 [27] is derived from the standard IEC 60034-18-21 [139] for round wire windings and the standard IEC 60034-18-31 [140] for windings with preformed elements. The test procedure is a comparative test in which the electrical insulation system under test is compared to a reference system as defined in standard IEC 60034-18-1 [141], where a sufficient amount of operating experience is available. Both systems are subjected to the same stress in the qualification test and the candidate system is qualified if it can withstand at least the same number of aging cycles without PDs below the specified threshold. The need for a reference system is criticized in [77].

According to the standard IEC 60034-18-21 [139] or IEC 60034-18-31 [140], at least five test specimens are required, the quality of which must be ensured by electrically suitable measurements and visual inspection before beginning. After that, prediagnostic tests are performed. Here, the specimens are subjected to maximal operating switching frequency and the test voltage according to Table 3 for 24 hours to ensure that the specimens have in principle the capability to withstand more than one aging cycle. The prediagnosis is also intended to provide information about possible heat generation during inverter feeding in the aging cycles. Failure during the prediagnosis is identical to the end criterion of PD occurrence below the test voltage. If passed, the specimens enter the cyclic sequence, which consists of a thermal aging subcycle, a conditioning subcycle, and the diagnostic test repeated in each cycle. The whole procedure is outlined in Fig. 18.

In the thermal aging cycle, the test specimens are stressed according to their designed thermal class with three different temperatures under controlled conditions, which are on average at least 10 K and at maximum 70 K above the temperature of their thermal class. The lower the temperature difference, the longer the duration (in days) of the aging cycle specified in the standard. The average lifetime at each aging temperature should be 10 cycles preferably, according to the standard. After completion of the aging subcycle, a defined exposure to humidity and mechanical stress takes place in the conditioning cycle to simulate environmental influences during real operation. For mechanical stress, the test objects are mounted on a shaker table and subjected to vibration at a frequency of 50 or 60 Hz for one hour. An acceleration of approximately 1.5 g is applied to the test specimen. The controlled exposure to humidity is realized with a climatic chamber. The humidity in it is 90% for 48 hours. The cycle ends with the diagnostic test, during which, in addition to a PD test, other informative measurements can be made from which the condition of the insulation can be deduced. For the measured variables, the aging indicators mentioned in Section IV-E can be considered. If the diagnostic test is not passed or if the insulation has already failed, the test process ends at this point. Due to the sequential nature of the test procedure, only an indirect interaction of factors can be accounted for [84].

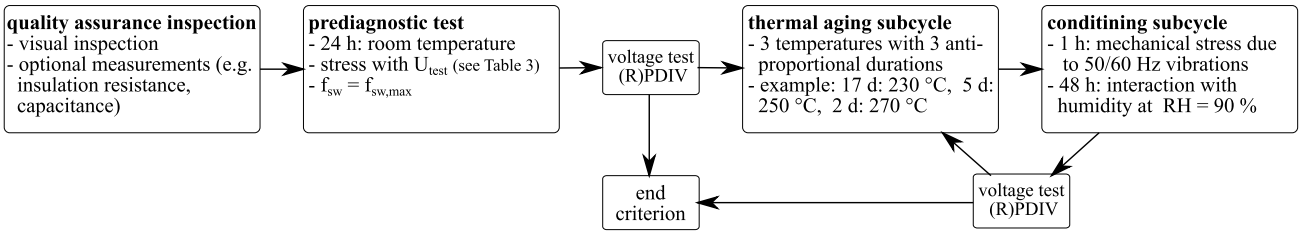

FIGURE 18. Schematic illustration of the cyclic test procedure according to the standard IEC 60034-18-41 [27].

E. MEASUREMENT, TEST SETUP, AND SPECIMEN

The aim is to generate data with the aid of suitable measurement methods, analyze them, and derive the aging state of the insulation from them. Furthermore, the measurement data can provide information about the remaining extrapolated lifetime to be expected [86]. In addition to measurements for diagnostic purposes, there are several tests that are used to inspect the quality of the insulation system [48]. Measurements carried out on a machine that is out of operation or on individual parts of a machine are referred to as ''offline measurements'', whereas values recorded during operation are referred to as ''online measurements'' or ''online monitoring'' [142].

In the context of investigations on LV machines, imitations of the insulation system in the form of wire pairs according to the standard IEC60851-5 [48], so-called motorettes/formettes (single- or three-phase) [90], [92], [119], [143], [144], [145] and rarely – due to the associated high costs – complete stators are used as test specimens [119], [146], [147], [148]. Many contributions concentrate on the component level of the materials used and other manufacturing parameters [44], [47], [91]. Specimens aside from the standard are also motivated [56], [90], [112]. To reduce the statistical sample dispersion, e.g. due to naturally manufacturing influences, test specimens of the same type are subjected to the same stress vectors in parallel. Depending on the theoretical distribution function used, the standard deviation, and the confidence level, the required number of specimens can be determined [135]. The standard IEC 6003418-32 [149] recommends at least five test specimens. In literature often no number of test specimens is mentioned so it can be assumed that only one test specimen was examined per test, whereas in the standard IEC 62539 [136] or IEC 60172 [133] a number of 10 is demanded. In paper [47] even a number of at least 15 is suggested. Wire pairs are used most frequently since they are cost-effective and easy to manufacture.

The specimens are subjected to electrical stress using either a commercial pulse or sinusoidal voltage generator [112], special surge voltage testers [47], or self-developed power electronics (half or full bridge) with SiC or gallium nitride (GaN) semiconductors [15], [73], which are the closest to real operation later. Each setup has different electrical characteristics, thus the comparability and reproducibility of the results are low. In addition, it is not clear how high the stress at the motor terminals will be in the real operation of the traction application [143]. Furthermore, available literature makes it difficult for the reader to make a well-founded classification or conclusion since it is often unclear at which point or under which conditions the measurements were made: motor terminals or at the power electronics, measured with or without a load. Moreover, it is not apparent from the measurement setup or with the data given, under which exact test conditions the tests took place: humidity information, heat development at the test specimen, manufacturing quality, fundamental information about the test specimen such as number, size, etc.

There are a variety of measurement methods for each voltage waveform (AC, DC, PV). Measuring PD activity or rather PD inception is the most important tool for determining the aging condition or for estimating the lifetime [19], [86], [142]. For this reason, a separate section is dedicated to this topic in the following. Other quantities listed below, can also provide information about the aging stage of the insulation system [19], [86], [142]:

- dissipation factor tan(δ)
- insulation capacitance C_I
- insulation resistance (IR)
- polarization index (PI)
- dielectric system response (in frequency/time domain)

1) PD MEASUREMENT

Regarding stress, AC, DC, and surge voltage measurements are considered separately. For surge/pulsed voltages, the characteristics of the surges/pulses (rise time, repetition rate, duration, form, polarity) influence the PD behavior. Like any measured quantity, PD measurements are subject to a measurement error due to the measuring device itself and environmental conditions. In addition to the properties of the specimens as well as the structure and materials of the insulation system, the measurement is influenced to a high degree by the environmental factors which are relevant for the discharge mechanisms (see Section III). Signals caused by internal PDs (see Section III-F) have rise times and pulse duration in the nanosecond range. So, the frequency spectrum extends extremely broad from radio frequency (RF: 3 – 30 MHz) to very high frequency (VHF: 30 – 300 MHz) to ultra-high frequency (UHF: 300 – 3000 MHz) [86], [87]. PD measurement distinguishes between electrical and non-electrical methods. Electrical and electromagnetic measurement methods are classified as follows:

- capacitive couplers
- inductive couplers
- electromagnetic sensors (antennas in the near-field)

Since the phenomenon of PD is associated with a large number of concomitant effects there is accordingly a range of measurement methods that can quantify these processes. This in turn leads to a variety of specialized disciplines, such as comparison of the different sensor types, noise suppression, pulse pattern classification as well as fault identification and location [19], [150], [151], [152]. The nonelectrical measurements can be divided into three categories:

- optical: measurements using UV cameras, IF thermal imaging camera, photomultiplier or image intensifier [73], [153]
- acoustical: detection using directional microphones or other acoustic transducers [153], [154], [155]
- chemical: measurement of ozone concentration in the air and chemical analysis of gaseous or liquid insulating materials [55], [153], [156].

The light emission, which in the case of PD extends from the infrared to the ultraviolet spectral range, enables the use of optical methods. Since PDs also produce acoustic emissions, these can be detected with suitable sensors in the liquid or gaseous medium. PDs in liquid or gaseous dielectrics also generate decomposition products, such as ozone, which can be detected with the aid of chemical analyses. They are relevant to the aging and condition of the insulation system as it is chemically attacked by them. [86].

Decades of research in HV technology have focused on the quantification of ''the'' PD quantity (see Table 4), which can provide insight into lifetime reduction or aging caused by PD in the insulation system. As of today, this goal has not been satisfactorily achieved, but the apparent charge q has become internationally established as ''the'' decisive measurand in the HV field [19], [86], [87]. In Table 4 further PD quantities can be found, which will also be discussed.

In conventional PD measurement, a high voltage is applied to the specimen and connected to a coupling capacitor, which acts as a high pass filter, and to a coupling device (CD) (see Fig. 12a) [157]. When the ignition voltage or breakdown voltage is exceeded, the cavity capacitance is discharged via the discharge path (D in Fig. 12a). The CD is then used to measure the current $i_{\mathrm{m}}(t)$ from the coupling capacitor, which recharges the cavity capacitance. Since the real charge q_{r} that is transferred in the cavity capacitance cannot be measured directly, the measured charge is referred to as the so-called apparent charge q. It is related to the real charge by the following formula, but the quotient of the series C_{s} and cavity capacitance C_{c} is unknown:

$$q = \Delta q_{\mathrm{r}} \cdot \frac{C_{\mathrm{s}}}{C_{\mathrm{c}}} \tag{26}$$

An advantage of measuring the apparent charge is the invariance concerning the pulse shape, which depends on the test and measurement setup and results from the integration of the current over time. Considering the complex frequency spectrum $F(j\omega)$ of a current pulse [86]:

$$F(j\omega) = \int_{t=-\infty}^{\infty} i(t) \cdot e^{-j\omega t}\,\mathrm{dt} \tag{27}$$

Then for $t > 0$ and $\omega = 0$ the identity of the apparent charge can be established:

$$q = \int_{t=0}^{\infty} i_{\mathrm{m}}(t)\,\mathrm{dt} = F(0) \tag{28}$$

Considering the magnitude response of a PD, it can be seen that $F(j\omega)$ still meets $F(0)$ for higher frequencies. This represents the operating principle of conventional PD charge measurement devices. The CD is a network with band-pass or high-pass behavior. Here, a distinction is made between narrow-band and wide-band measuring devices and between ''real'' and quasi-integration. When integrating the PD pulse with narrow-band (4 kHz – 10 kHz) or wide-band (100 kHz – 500 kHz) measuring instruments in the frequency domain, the integration is a quasi-integration. In the case of an analog circuit or a computer-aided electronic circuit, the actual time curve of the PD is integrated. In addition to these fairly low-frequency measurements, which are covered up to 1 MHz by the IEC 60270 standard [157], unconventional measurements are also undertaken in the HF, VHF, and UHF ranges, since the spectrum of PD extends far into the GHz range. Measurements in the UHF are the preferred choice since a large number of known narrow-band interference sources (e.g., cellular telephony or television) can be suppressed with an appropriate high-pass filter (HPF). A disadvantage is that the apparent charge cannot be measured directly, but only estimated by comparative measurement. Solely a synchronous multichannel measurement establishes a direct relationship between the UHF measurement and the apparent charge [19].

The above measurement methods can be used for both AC and DC. However, PD pulses occur less frequently and more irregularly with DC, since only a very small conduction current in relation to the displacement current at AC recharges the fault. Thus, with DC, there is no continuous charge flow. Instead, long measurements are required during which the charge and the number of pulses have to be recorded. DC measurements are more susceptible to external interference, and a high level of interference suppression and shielding is required [19], [86]. In classical PD diagnosis with AC in the HV field, the apparent charge together with empirical values serves as a measure of PD deterioration and threshold values can be defined. PDIV and PDEV serve as indicators of manufacturing defects, and the phase angle provides information on the type and location of the discharge [19], [86], [158]. To complete the overall picture of PD measurement technology at this point, reference should also be made to advanced PD measurement methods that offer extensive visualization and evaluation possibilities through digital data processing. Two- or three-dimensional

TABLE 4. PD quantities in AC, DC, and PV regime.

PD quantities	symbol	equation	SI unit	applicability
pulse count	m	$\sum_{\Delta t}$ pulses		AC,DC, PV
pulse repetition rate	n	$\frac{\text{pulses}}{\Delta t}$	s^{-1}	AC, DC, PV
pulse repetition frequency	N	$\frac{\text{pulses}}{1\cdot\text{s}}$	s^{-1}	AC, DC, PV
pulse count per switching		$\sum_{T}$ pulses	s^{-1}	AC,DC, PV
phase angle (to test voltage)	ϕ_i/φ	$360^\circ\cdot\frac{t_i}{T}$	$^\circ$	AC
apparent charge	q/Q	$\int_0^\infty i_\text{m}(t)\,\text{dt}$	C	AC, DC
discharge energy	W_PD	$\frac{1}{2}\,q\,\sqrt{2}\,\text{PDIV}$	J	AC, DC
accumulated apparent charge	q_a	$\sum_i q_i$	C	AC, DC
average discharge current	I	$\frac{1}{\Delta t}\sum_i \lvert q_i\rvert$	A	AC, DC
discharge power	P	$\frac{1}{\Delta t}\sum_i q_i\cdot u_i$	W	AC, DC
quadratic rate	D	$\frac{1}{\Delta t}\sum_i q_i^2$	$\text{C}^2\,\text{s}^{-1}$	AC, DC
inception voltage	PDIV		V	AC, DC, (PV)
extinction voltage	PDEV		V	AC, DC, (PV)
magnitude	U_m		V	AC, DC, PV
peak magnitude	$\hat{U}_\text{m}$		V	AC, DC, PV
repeatedly peak magnitude	$\hat{U}_\text{rm}$		V	AC, PV
repeatedly inception voltage	RPDIV		V	PV
repeatedly extinction voltage	RPDEV		V	PV

indices: i = running index, a = accumulated, m = measured, rm = repeatedly measured

phase-resolved histogram-like ϕ,q,n-representations (PRPD pattern) and star/relation diagrams, which can be graphically constructed by different types of synchronous multichannel measurement (three-phase amplitude relation diagram (3PARD), three-phase time relation diagram (3PTRD), three-channel frequency relation diagram (3CFRD)), should be mentioned [19], [86], [159], [160]. Some exemplary measurement results shown in such diagrams are shown in Fig. 19.

Special requirements have to be met by PD measurement systems for pulsed voltage stresses since fast voltage pulses are associated with the emission of strong electromagnetic radiation and thus disturb the PD measurement due to superimposed spectral components. Instead of a simple HPF (coupling capacitor), which is sufficient for AC stress, high-order (active) HPF, high-frequency current transformers (HFCT) with multipole filter, ultra-wideband (UWB) directional couplers with HPF, or narrow-band UHF antennas are used. All of these are capable of sufficiently suppressing the frequency components caused by the pulsed voltage itself [162]. The apparent charge cannot be determined for pulsed voltages. The PD measurement values for pulsed voltages depend on the sensitivity of the measurement system and setup and can therefore not universally be compared. In literature, the efforts of interference suppression in the study of wire pairs range from very low [46] to very high [73].

Measurement problems include the high sensitivity of PD charges in the pC range to test setup induced, external electromagnetic, and line disturbances. Pulsed voltages increase the measurement uncertainty due to interference. The interpretation of the measurement data can also prove to be difficult.

2) STATISTICAL SIZE EFFECTS – ENLARGEMENT LAWS

Statistical laws are known from HV technology concerning values determined or derived from tests, such as the breakdown field strength and lifetime values, which also apply to LV machines. The following effects occur because tests are usually only performed on imitations or partial elements of the insulation system due to cost and practical reasons. Therefore, when evaluating the data, the following effects should always be kept in mind and included in the consideration [19], [87], [135]:

- area effect
- volume effect
- parallelism effect
- time effect

Depending on the degree of uniformity of the field distribution, an area or volume effect exists with the practical application of the multiplication law for independent probabilities in discharge mechanisms. This states that an increase in the electrode area or an increase in the stressed insulation volume

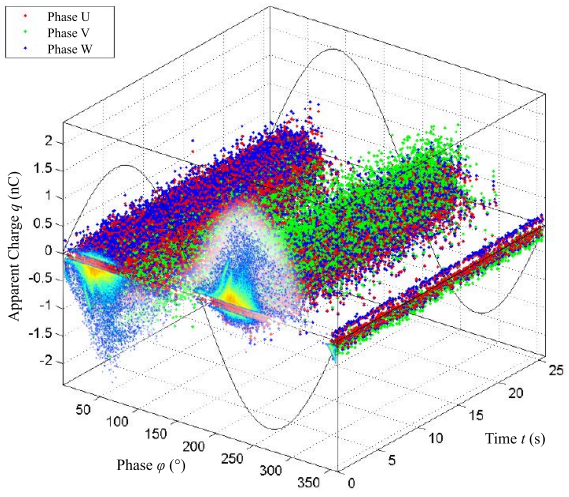

(a) Exemplary 3D PRPD pattern [160]

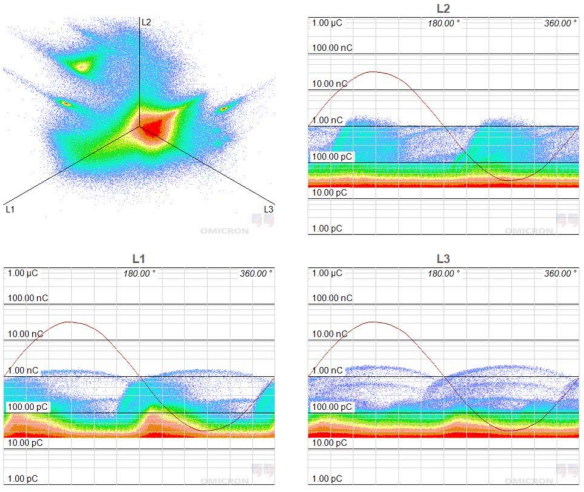

(b) Exemplary three-phase relation diagram and 2D PRPD [161]

FIGURE 19. Advanced PD measurement methods.

has the effect, that the electrical resilience reduces. Parallel processes also have a statistical effect, that the resilience is reduced. They are described by the parallelism effect, which occurs for example in multiphase rotating machines, which have parallel coil branches per phase. The resilience of the overall arrangement is determined by the point at which the discharge has built up most quickly in the random process. The last effect to be mentioned is the time effect, which is to be expected for impulse stresses. If damage accumulation is assumed to have not yet started, the discharge process is largely determined by random influences (e.g., presence of a start electron), therefore increasing stress duration is accompanied by a resilience reduction [19], [87], [135].

V. CONCLUSION

In this paper, available literature was consulted with reference to HV technology/engineering to give a review about the state-of-the-art and the current challenges in insulation systems for LV motors in the automotive field. For this purpose, the design features of the insulation system in LV machines were addressed and a comparison with HV machines was carried out. Here, the hairpin winding for traction motors, which satisfies the special automotive requirements very well, takes on a special role, since investigations in the past have almost exclusively referred to random wound windings.

The discharge behavior of an insulation arrangement determines its electrical resilience and reliability. Thus, the physics of the discharge processes is essential for the evaluation. Hence, the physical interactions were represented by a relation structure of domains of the insulation system. Here, the phenomenon of PD plays a central role, therefore a detailed description was given. The dynamic and static description of discharges in solid and gaseous dielectrics was motivated by established physical modeling from HV technology, as these can also be applied to LV machines. Despite the well-known physical modeling, a satisfactory prediction accuracy for the lifetime has not yet been achieved in literature. Often, experimental data collection is used to attempt to derive findings about the level of degradation as a function of the stress parameters.

Finally, in the fourth section, aging and the lifetime predictions deduced therefrom were described with reference to accelerated aging tests and the relevant standards. The electrical factors that influence aging and the quantities that can serve as indicators of aging were considered in order to be able to adapt empirical or physical models for lifetime estimation. In addition, statistics, having an important role, were described. Since the insulation field of insulation characterization/design and lifetime assessment has a high experimental character, the measurement techniques of PDs were also addressed. Overall, there has been a high number of published articles recently, but with contradictory results, also in connection with other TEAM factors. Different test specimens and measurement setups lead to the fact that the measurement results cannot be compared, a scientific discussion becomes at least difficult and a derivation of design guidelines based on currently available literature seems impossible. Furthermore, PD measurement methods established for AC voltage from HV technology cannot be applied directly.

In summary, due to the interdisciplinary nature and complexity of the currently reported insulation problems in LV inverter-fed motors, dissent still clearly outweighs consensus, so a considerable research effort remains necessary.

We will utilize the knowledge and gained findings compiled in this article to publish further studies on this topic.

REFERENCES

[1] A. M. Andwari, A. Pesiridis, S. Rajoo, R. Martinez-Botas, and V. Esfahanian, "A review of battery electric vehicle technology and readiness levels," *Renew. Sustain. Energy Rev.*, vol. 78, pp. 414–430, Oct. 2017.

[2] K. Bae, R. Plikat, C. Besch, Z. Neuschl, B. Gaussens, M. Bailoni, A. Litinsky, F. Saborowski, and M. Kurrat, "Current state and development trends of insulation systems in BEV traction motors steered by electric powertrain innovation," in *Proc. PCIM Eur. Digit. Days*, 2021, pp. 1–8.

[3] M. Kaufhold, G. Borner, M. Eberhardt, and J. Speck, "Failure mechanism of the interturn insulation of low voltage electric machines fed by pulse-controlled inverters," *IEEE Electr. Insul. Mag.*, vol. 12, no. 5, pp. 9–16, Sep. 1996.
[4] D. Fabiani, "Accelerated degradation of AC motor insulation due to voltage waveforms generated by adjustable speed drives," Ph.D. dissertation, Dipartimento di Ingegneria Elettrica, Univ. Bologna, Bologna, Italy, 2003.
[5] A. Cavallini, D. Fabiani, and G. Montanari, "Power electronics and electrical insulation systems—Part 1: Phenomenology overview," *IEEE Elect. Insul. Mag.*, vol. 26, no. 3, pp. 7–15, May 2010.
[6] Y. Ji, P. Giangrande, V. Madonna, W. Zhao, and M. Galea, "Reliability-oriented design of inverter-fed low-voltage electrical machines: Potential solutions," *Energies*, vol. 14, no. 14, p. 4144, Jul. 2021.
[7] P. J. Tavner, "Review of condition monitoring of rotating electrical machines," *IET Electr. Power Appl.*, vol. 2, no. 4, p. 215, 2008.
[8] A. H. Bonnett and C. Yung, "Increased efficiency versus increased reliability," *IEEE Ind. Appl. Mag.*, vol. 14, no. 1, pp. 29–36, Jan./Feb. 2008.
[9] A. Siddique, G. S. Yadava, and B. Singh, "A review of stator fault monitoring techniques of induction motors," *IEEE Trans. Energy Convers.*, vol. 20, no. 1, pp. 106–114, Mar. 2005.
[10] M. Keller, M. Maier, T. Petri, and N. Parspour, "Modelling the dynamic voltage distribution in electric traction motor windings," in *Proc. Int. Symp. Power Electron., Electr. Drives, Autom. Motion (SPEEDAM)*, Jun. 2022, pp. 599–604.
[11] C.-N. Behrendt, J. Dittmann, B. Knebusch, and B. Ponick, "Common-mode impedance prediction of a high frequency hairpin stator winding based on FEM and modified nodal analysis," in *Proc. Int. Symp. Power Electron., Electr. Drives, Autom. Motion (SPEEDAM)*, Jun. 2022, pp. 20–26.
[12] L. V. Hanisch, L. Eisele, K. Lünne, and M. Henke, "Modeling of transient overvoltages in inverter-fed machines with hairpin winding," in *Proc. Int. Symp. Power Electron., Electr. Drives, Autom. Motion (SPEEDAM)*, Jun. 2022, pp. 605–609.
[13] S. Sundeep, J. Wang, A. Griffo, and F. Alvarez-Gonzalez, "Peak voltage stress on stator winding in PWM inverter fed drives," in *Proc. Int. Conf. Electr. Mach. (ICEM)*, Aug. 2020, pp. 1579–1585.
[14] X. Ju, Y. Cheng, M. Yang, S. Cui, A. Sun, X. Liu, and M. He, "Voltage stress calculation and measurement for hairpin winding of EV traction machines driven by SiC MOSFET," *IEEE Trans. Ind. Electron.*, vol. 69, no. 9, pp. 8803–8814, Sep. 2022.
[15] L. Hanisch, M. Sun, and M. Henke, "Novel modeling approach for voltage distribution within automotive electrical machines," in *Proc. Int. Conf. Electr. Mach. (ICEM)*, Aug. 2020, pp. 2196–2201.
[16] F. Pauli, Y. Wu, N. Driendl, M. Schröder, and K. Hameyer, "Transiente spannungsmodellierung in umrichtergespeisten niederspannungsmaschinen mit steckwicklungen," *Elektrotechnik Informationstechnik*, vol. 137, nos. 4–5, pp. 179–187, Aug. 2020.
[17] C. Jung, "Power up with 800-V systems: The benefits of upgrading voltage power for battery-electric passenger vehicles," *IEEE Electrific. Mag.*, vol. 5, no. 1, pp. 53–58, Mar. 2017.
[18] M. Doppelbauer, *Grundlagen der Elektromobilität*. Wiesbaden, Germany: Springer, 2020.
[19] A. Küchler, *High Voltage Engineering*. Berlin, Germany: Springer, 2018.
[20] E. Kuffel, J. Kuffel, and W. S. Zaengl, *High Voltage Engineering: Fundamentals*, 2nd ed. London, U.K.: Newnes, 2000.
[21] J. S. Pearson, O. Farish, B. F. Hampton, M. D. Judd, D. Templeton, B. W. Pryor, and I. M. Welch, "Partial discharge diagnostics for gas insulated substations," *IEEE Trans. Dielectr. Electr. Insul.*, vol. 2, no. 5, pp. 893–905, Oct. 1995.
[22] E. A. Boulter and G. C. Stone, "Historical development of rotor and stator winding insulation materials and systems," *IEEE Electr. Insul. Mag.*, vol. 20, no. 3, pp. 25–39, May/Jun. 2004.
[23] G. C. Stone, *Electrical Insulation for Rotating Machines: Design, Evaluation, Aging, Testing, and Repair* (IEEE Press Series on Power Engineering), vol. 8, 2nd ed. Hoboken, NJ, USA: Wiley, 2014.
[24] G. Müller, K. Vogt, and B. Ponick, *Berechnung Elektrischer Maschinen* (Wiley Interscience Online Books), 6th ed. Hoboken, NJ, USA: Wiley, 2008.
[25] P. Stenzel, "Großserientaugliche nadelwickeltechnik für verteilte wicklungen im anwendungsfall der e-traktionsantriebe," Ph.D. dissertation, Lehrstuhl für Fertigungsautomatisierung und Produktionssystematik, Friedrich-Alexander-Universität Erlangen-Nürnberg, Meisenbach KG, Erlangen, Germany, 2017.
[26] P. L. Herrmann, "Automatisierte trajektorienplanung für die nadelwickeltechnik," Ph.D. dissertation, Lehrstuhl für Elektrische Antriebssysteme und Leistungselektronik, Technischen Universität München, Munich, Germany, 2021.
[27] *Rotating Electrical Machines—Part 18–41: Partial Discharge Free Electrical Insulation Systems (Type I) Used in Rotating Electrical Machines Fed From Voltage Converters—Qualification and Quality Control Tests*, Standard IEC 60034-18-41, 2020.
[28] *IEC Standard Voltages*, Standard IEC 60038, 2011.
[29] *High-Voltage Test Techniques—Part 1: General Definitions and Test Requirements*, Standard IEC 60060-1, 2010.
[30] A. Riedel, M. Masuch, M. Weigelt, T. Glassel, A. Kuhl, S. Reinstein, and J. Franke, "Challenges of the hairpin technology for production techniques," in *Proc. 21st Int. Conf. Electr. Mach. Syst. (ICEMS)*, Oct. 2018, pp. 2471–2476.
[31] Y. Zhao, D. Li, T. Pei, and R. Qu, "Overview of the rectangular wire windings AC electrical machine," *CES Trans. Electr. Mach. Syst.*, vol. 3, no. 2, pp. 160–169, Jun. 2019.
[32] T. Glaessel, D. B. Pinhal, M. Masuch, D. Gerling, and J. Franke, "Manufacturing influences on the motor performance of traction drives with hairpin winding," in *Proc. 9th Int. Electr. Drives Prod. Conf. (EDPC)*, Dec. 2019, pp. 1–8.
[33] A. Ruf, "Thermische ausnutzung von elektrischen Maschinen unter berücksichtigung der lebensdauer am beispiel eines traktionsantriebs," Ph.D. dissertation, Institut für Elektrische Maschinen, RWTH Aachen, Aachen, Germany, 2018.
[34] M. Szczepanski, "Development of methods allowing the test and the comparison of low-voltage motors insulation systems running under partial discharges (fed by inverter)," Ph.D. dissertation, Laboratoire Plasma et Convers. d'Energie, Université Paul Sabatier Toulouse III, Toulouse, France, 2019.
[35] L. Benmamas, "Méthodes d'évaluation du risque de décharges partielles dans le bobinage de machines électriques destinées à la traction automobile," Ph.D. dissertation, GeePs—Laboratoire Génie Électrique et Électronique de Paris, Université Paris Saclay, Paris, France, 2018.
[36] *Electrical Insulation—Thermal Evaluation and Designation*, Standard IEC 60085, 2008.
[37] *Electrical Insulating Materials—Thermal Endurance Properties—Part 1: Ageing Procedures and Evaluation of Test Results*, Standard IEC 60216-1, 2013.
[38] *Specifications for Particular Types of Winding Wires—Part 0–1: General Requirements—Enamelled Round Copper Wire*, Standard IEC 60317-0-1, 2019.
[39] *Rotating Electrical Machines—Part 6: Methods of Cooling*, Standard IEC 60034-6, 1993.
[40] G. Müller and B. Ponick, *Grundlagen Elektrischer Maschinen* (Elektrische Maschinen), 10th ed. Hoboken, NJ, USA: Wiley, 2014.
[41] M. Halwas, F. S.-L. Blanc, B. Jux, M. Doppelbauer, F. Wirth, L. Hausmann, J. Hofmann, and J. Fleischer, "Coherences between production technology and performance of electric traction drives," in *Proc. 9th Int. Electr. Drives Prod. Conf. (EDPC)*, Dec. 2019, pp. 1–9.
[42] C. V. Maughan, "A 100-year history of generator insulation systems," *IEEE Electr. Insul. Mag.*, vol. 34, no. 4, pp. 42–53, Jul. 2018.
[43] L. Lusuardi, A. Rumi, A. Cavallini, D. Barater, and S. Nuzzo, "Partial discharge phenomena in electrical machines for the more electrical aircraft. Part II: Impact of reduced pressures and wide bandgap devices," *IEEE Access*, vol. 9, pp. 27485–27495, 2021.
[44] V. Grau and R. W. De Doncker, "The effects of steep voltage slopes on insulation systems of coil windings caused by next generation power semiconductor devices," in *Proc. IEEE Electr. Insul. Conf. (EIC)*, Jun. 2019, pp. 26–29.
[45] N. Driendl, F. Pauli, and K. Hameyer, "Modeling of partial discharge processes in winding insulation of low-voltage electrical machines supplied by high du/dt inverters," in *Proc. 45th Annu. Conf. IEEE Ind. Electron. Soc. (IECON)*, Oct. 2019, pp. 7102–7107.
[46] F. Pauli, N. Driendl, and K. Hameyer, "Study on temperature dependence of partial discharge in low voltage traction drives," in *Proc. IEEE Workshop Electr. Mach. Design, Control Diagnosis (WEMDCD)*, Apr. 2019, pp. 209–214.
[47] K. Hameyer, A. Ruf, and F. Pauli, "Influence of fast switching semiconductors on the winding insulation system of electrical machines," in *Proc. Int. Power Electron. Conf. (IPEC-Niigata ECCE Asia)*, May 2018, pp. 740–745.

[48] *Winding Wires—Test Methods—Part 5: Electrical Properties*, Standard IEC 60851-5, 2019.

[49] L. Lusuardi, "Towards a partial discharge free insulation system for the more electrical transportation," Ph.D. dissertation, Dept. Elect., Electron. Inf. Eng., Università di Bologna, Bologna, Italy, 2020.

[50] M. Chapman, N. Frost, and R. Bruetsch, "Insulation systems for rotating low-voltage machines," in *Proc. IEEE Int. Symp. Electr. Insul.*, Jun. 2008, pp. 257–260.

[51] M. Halwas, L. Hausmann, F. Wirth, J. Fleischer, B. Jux, and M. Doppelbauer, "Influences of design and manufacturing on the performance of electric traction drives," in *Proc. Int. Conf. Electr. Mach. (ICEM)*, Aug. 2020, pp. 488–494.

[52] F. Senn, "Untersuchung elektrisch halbleitender Materialien für den einsatz in glimmschutzsystemen rotierender hochspannungsmaschinen," Ph.D. dissertation, Institut für Hochspannungstechnik und Systemmanag., Technische Universität Graz, Graz, Austria, 2010.

[53] T. Brügger, "Einfluss starker lastwechseldynamik auf das alterungsverhalten der isolierung grosser hydrogeneratoren," Ph.D. dissertation, Institut für Elektrische Energieübertragung und Hochspannungstechnik, ETH Zürich, Zürich, Switzerland, 2011.

[54] H. Sequenz, M. Brüderlink, E. Feiten, O. Haus, R. Knobloch, D. Lambrecht, F. Maier, W. Mertens, G. Neidhöfer, W. Oburger, and A. Wichmann, *Herstellung der Wicklungen Elektrischer Maschinen*. Vienna, Austria: Springer, 1973.

[55] G. C. Stone, "Advancements during the past quarter century in on-line monitoring of motor and generator winding insulation," *IEEE Trans. Dielectr. Electr. Insul.*, vol. 9, no. 5, pp. 746–751, Oct. 2002.

[56] F. Pauli, M. Kilper, N. Driendl, and K. Hameyer, "Modeling of the partial discharge process between the winding and the stator of low voltage machines for traction applications," *IEEE Trans. Energy Convers.*, vol. 36, no. 3, pp. 2310–2318, Sep. 2021.

[57] J. S. Townsend, "The conductivity produced in gases by the motion of negatively-charged ions," *Nature*, vol. 62, no. 1606, pp. 340–341, Aug. 1900.

[58] R. Clausius, "X. On the mean length of the paths described by the separate molecules of gaseous bodies on the occurrence of molecular motion: Together with some other remarks upon the mechanical theory of heat," *London, Edinburgh, Dublin Phil. Mag. J. Sci.*, vol. 17, no. 112, pp. 81–91, Feb. 1859.

[59] F. Paschen, "Ueber die zum funkenübergang in luft, Wasserstoff und kohlensäure bei verschiedenen drucken erforderliche potentialdifferenz," *Ann. Phys.*, vol. 273, no. 5, pp. 69–96, 1889.

[60] P. Hartherz, *Anwendung der Teilentladungsmeßtechnik zur Fehleranalyse in Festen Isolierungen Unter Periodischer Impulsspannungsbelastung* (Berichte aus der Elektrotechnik). Herzogenrath, Germany: Shaker Verlag, 2002.

[61] K. Ollegott, P. Wirth, C. Oberste-Beulmann, P. Awakowicz, and M. Muhler, "Fundamental properties and applications of dielectric barrier discharges in plasma-catalytic processes at atmospheric pressure," *Chem. Ingenieur Technik*, vol. 92, no. 10, pp. 1542–1558, Oct. 2020.

[62] N. Hayakawa and H. Okubo, "Partial discharge characteristics of inverter-fed motor coil samples under ac and surge voltage conditions," *IEEE Electr. Insul. Mag.*, vol. 21, no. 1, pp. 5–10, Jan. 2005.

[63] D. Muto, M. Oya, T. Aoi, and T. Ueno, "A study on partial discharge phenomena of winding wires," in *Furukawa Rev.*, vol. 45, pp. 13–21, Jul. 2014.

[64] P. Collin, D. Malec, and Y. Lefevre, "About the relevance of using Paschen's criterion for partial discharges inception voltage (PDIV) estimation when designing the electrical insulation system of inverter fed motors," in *Proc. IEEE Electr. Insul. Conf. (EIC)*, Jun. 2019, pp. 513–516.

[65] I. Cotton, R. Gardner, D. Schweickart, D. Grosean, and C. Severns, "Design considerations for higher electrical power system voltages in aerospace vehicles," in *Proc. IEEE Int. Power Modulator High Voltage Conf. (IPMHVC)*, Jul. 2016, pp. 57–61.

[66] L. Benmamas, P. Teste, G. Krebs, E. Odic, F. Vangraefschepe, and T. Hamiti, "Contribution to partial discharge analysis in inverter-fed motor windings for automotive application," in *Proc. IEEE Electr. Insul. Conf. (EIC)*, Jun. 2017, pp. 348–351.

[67] M. Kaufhold, H. Aninger, M. Berth, J. Speck, and M. Eberhardt, "Electrical stress and failure mechanism of the winding insulation in PWM-inverter-fed low-voltage induction motors," *IEEE Trans. Ind. Electron.*, vol. 47, no. 2, pp. 396–402, Apr. 2000.

[68] M. G. L. De Calle, J. M. Martinez-Tarifa, A. M. G. Solanilla, and G. Robles, "Uncertainty sources in the estimation of the partial discharge inception voltage in turn-to-turn insulation systems," *IEEE Access*, vol. 8, pp. 157510–157519, 2020.

[69] A. Hopf, "Elektrische festigkeit von SF_6 und alternativen isoliergasen (luft, CO_2, N_2, O_2 und C_3F_7CN-gemisch) bis 2,6 MPa," Ph.D. dissertation, Fachgebiet Elektrische Geräte und Anlagen, Technischen Universität Ilmenau, Ilmenau, Germany, 2020.

[70] H. Raether, *Electron Avalanches and Breakdown in Gases*. Washington, DC, USA: Butterworth, 1964.

[71] A. Chvyreva, S. Pancheshnyi, T. Christen, and A. J. M. Pemen, "Raether–Meek criterion for prediction of electrodeless discharge inception on a dielectric surface in different gases," *J. Phys. D, Appl. Phys.*, vol. 51, no. 11, Mar. 2018, Art. no. 115202.

[72] A. Schwaiger, *Elektrische Festigkeitslehre*. Berlin, Germany: Springer, 1925.

[73] V. Grau, "Development of a test bench to investigate the impact of steep voltage slopes on the lifetime of insulation systems for coil windings," Ph.D. dissertation, Institut für Elektrische Maschinen, RWTH Aachen, Aachen, Germany, 2021.

[74] G. W. Trichel, "The mechanism of the negative point to plane corona near onset," *Phys. Rev.*, vol. 54, pp. 1078–1084, Dec. 1938.

[75] G. C. Montanari, "Bringing an insulation to failure: The role of space charge," *IEEE Trans. Dielectr. Electr. Insul.*, vol. 18, no. 2, pp. 339–364, Apr. 2011.

[76] D. Fabiani, G. C. Montanari, A. Cavallini, and G. Mazzanti, "Relation between space charge accumulation and partial discharge activity in enameled wires under PWM-like voltage waveforms," *IEEE Trans. Dielectr. Electr. Insul.*, vol. 11, no. 3, pp. 193–205, Jun. 2004.

[77] A. Cavallini, "Reliability of low voltage inverter-fed motors: What have we learned, perspectives, open points," in *Proc. Int. Symp. Electr. Insulating Mater. (ISEIM)*, Sep. 2017, pp. 13–22.

[78] K. Kimura, S. Itaya, S. Ushirone, M. Hikita, and W. Bito, "Discharge condition and surface charge distribution under repetitive bipolar impulses," in *Proc. IEEE 7th Int. Conf. Properties Appl. Dielectr. Mater.*, Jun. 2003, pp. 1061–1064.

[79] N. Hayakawa, F. Shimizu, and H. Okubo, "Estimation of partial discharge inception voltage of magnet wires under inverter surge voltage by volume-time theory," *IEEE Trans. Dielectr. Electr. Insul.*, vol. 19, no. 2, pp. 550–557, Apr. 2012.

[80] D. Kind, M. Kurrat, and T. H. Kopp, "Voltage-time characteristics of air gaps and insulation coordination—Survey of 100 years research," in *Proc. 33rd Int. Conf. Lightning Protection (ICLP)*, Sep. 2016, pp. 1–8.

[81] L. A. Dissado, G. Mazzanti, and G. C. Montanari, "The role of trapped space charges in the electrical aging of insulating materials," *IEEE Trans. Dielectr. Electr. Insul.*, vol. 4, no. 5, pp. 496–506, Oct. 1997.

[82] L. A. Dissado, "Understanding electrical trees in solids: From experiment to theory," *IEEE Trans. Dielectr. Electr. Insul.*, vol. 9, no. 4, pp. 483–497, Aug. 2002.

[83] P. H. F. Morshuis, "Degradation of solid dielectrics due to internal partial discharge: Some thoughts on progress made and where to go now," *IEEE Trans. Dielectr. Electr. Insul.*, vol. 12, no. 5, pp. 905–913, Oct. 2005.

[84] *Evaluation and Qualification of Electrical Insulation Systems*, Standard IEC 60505, 2011.

[85] G. C. Montanari and P. H. F. Morshuis, "Space charge phenomenology in polymeric insulating materials," *IEEE Trans. Dielectr. Electr. Insul.*, vol. 12, no. 4, pp. 754–767, Aug. 2005.

[86] K. Schon, *High Voltage Measurement Techniques*. Cham, Switzerland: Springer, 2019.

[87] W. Hauschild and E. Lemke, *High-Voltage Test and Measuring Techniques*. Cham, Switzerland: Springer, 2019.

[88] A. Pedersen, "Partial discharges in voids in solid dielectrics. An alternative approach," in *Proc. Conf. Electr. Insul. Dielectr. Phenomena Annu. Rep.*, Oct. 1987, pp. 58–64.

[89] M. R. Khowja, G. Turabee, P. Giangrande, V. Madonna, G. Cosma, G. Vakil, C. Gerada, and M. Galea, "Lifetime estimation of enameled wires under accelerated thermal aging using curve fitting methods," *IEEE Access*, vol. 9, pp. 18993–19003, 2021.

[90] L. V. Hanisch, T.-H. Dietrich, and M. Henke, "Analysis of partial discharges and failure mechanism in electrical machines with hairpin winding," in *Proc. IEEE 13th Int. Symp. Diag. Electr. Mach., Power Electron. Drives (SDEMPED)*, Aug. 2021, pp. 1–7.

[91] M. Kilper, M. Baader, H. Naumoski, and K. Hameyer, "Study on different partial discharge testing methods qualifying insulation materials for automotive applications," in *Proc. 10th Int. Electr. Drives Prod. Conf. (EDPC)*, Dec. 2020, pp. 1–6.
[92] P. Mancinelli, S. Stagnitta, and A. Cavallini, "Lifetime analysis of an automotive electrical motor with hairpin wound stator," in *Proc. IEEE Conf. Electr. Insul. Dielectr. Phenomena (CEIDP)*, Oct. 2016, pp. 877–880.
[93] P. Mancinelli, S. Stagnitta, and A. Cavallini, "Qualification of hairpin motors insulation for automotive applications," *IEEE Trans. Ind. Appl.*, vol. 53, no. 3, pp. 3110–3118, May 2017.
[94] C. He, C. P. Beura, and S. Tenbohlen, "Investigation of partial discharge activity in the slot of a hairpin-wound stator," in *Proc. Int. Symp. Electr. Insulating Mater. (ISEIM)*, 2020, pp. 565–568.
[95] L. A. Escobar and W. Q. Meeker, "A review of accelerated test models," *Stat. Sci.*, vol. 21, no. 4, pp. 552–577, Nov. 2006.
[96] A. C. Gjerde, "Multifactor ageing models—Origin and similarities," *IEEE Electr. Insul. Mag.*, vol. 13, no. 1, pp. 6–13, Jan./Feb. 1997.
[97] G. C. Montanari and L. Simoni, "Aging phenomenology and modeling," *IEEE Trans. Dielectr. Electr. Insul.*, vol. 28, no. 5, pp. 755–776, Oct. 1993.
[98] B. Sarlioglu and C. T. Morris, "More electric aircraft: Review, challenges, and opportunities for commercial transport aircraft," *IEEE Trans. Transport. Electrific.*, vol. 1, no. 1, pp. 54–64, Jun. 2015.
[99] V. Madonna, P. Giangrande, and M. Galea, "Electrical power generation in aircraft: Review, challenges, and opportunities," *IEEE Trans. Transport. Electrific.*, vol. 4, no. 3, pp. 646–659, Sep. 2018.
[100] G. Pietrini, D. Barater, G. Franceschini, P. Mancinelli, and A. Cavallini, "An open problem for more electrical aircraft (MEA): How insulation systems of actuators can be qualified?" in *Proc. IEEE Energy Convers. Congr. Expo. (ECCE)*, Sep. 2016, pp. 1–8.
[101] A. Ruf, F. Pauli, M. Schröder, and K. Hameyer, "Lebensdauermodellierung von nicht-teilentladungsresistenten isoliersystemen elektrischer Maschinen in dynamischen lastkollektiven," *Elektrotechnik und Informationstechnik*, vol. 135, no. 2, pp. 131–144, Apr. 2018.
[102] M. Fuerst and M.-M. Bakran, "Influence of the PWM voltage waveform on partial discharge occurrence in motor windings," in *Proc. PCIM Eur. Digit. Days*, 2020, pp. 1238–1245.
[103] Z. Wei, H. You, B. Hu, R. Na, and J. Wang, "Partial discharge behavior on twisted pair under ultra-short rise time square-wave excitations," in *Proc. IEEE Electr. Insul. Conf. (EIC)*, Jun. 2019, pp. 493–496.
[104] S. Matsumoto, N. N. Nam, D. Nagaba, and T. Ogiya, "Partial discharge characteristics of twisted magnet wire under high frequency AC voltage," in *Proc. Int. Symp. Electr. Insulating Mater.*, Jun. 2014, pp. 57–60.
[105] D. R. Meyer, A. Cavallini, L. Lusuardi, D. Barater, G. Pietrini, and A. Soldati, "Influence of impulse voltage repetition frequency on RPDIV in partial vacuum," *IEEE Trans. Dielectr. Electr. Insul.*, vol. 25, no. 3, pp. 873–882, Jun. 2018.
[106] P. Wang, H. Xu, J. Wang, A. Cavallini, and G. C. Montanari, "Temperature effects on PD statistics and endurance of inverter-fed motor insulation under repetitive square wave voltages," in *Proc. IEEE Electr. Insul. Conf. (EIC)*, Jun. 2016, pp. 202–205.
[107] P. Wang and A. Cavallini, "The influence of repetitive square wave voltage parameters on PD statistical features," in *Proc. Annu. Rep. Conf. Electr. Insul. Dielectr. Phenomena (CEIDP)*, Oct. 2013, pp. 1282–1285.
[108] N. Hayakawa, M. Morikawa, and H. Okubo, "Partial discharge inception and propagation characteristics of magnet wire for inverter-fed motor under surge voltage application," *IEEE Trans. Dielectr. Electr. Insul.*, vol. 14, no. 1, pp. 39–45, Feb. 2007.
[109] K. Kadowaki, Y. Takemura, and R. Ozaki, "Influence of very fast voltage-oscillation with polarity reversalon partial discharge inception probability for twisted enameled-wires," *Int. J. Electr. Eng. Informat.*, vol. 5, no. 1, pp. 45–54, Mar. 2013.
[110] P. Wang, M. Zhao, Q. Zhou, and J. Zhang, "The influence of SPWM frequency on the endurance of inverter-fed motor insulation," in *Proc. IEEE Conf. Electr. Insul. Dielectr. Phenomena (CEIDP)*, Oct. 2019, pp. 142–145.
[111] T. J. Å. Hammarström, "Partial discharge characteristics within motor insulatioi exposed to multi-level PWM waveforms," *IEEE Trans. Dielectr. Electr. Insul.*, vol. 25, no. 2, pp. 559–567, Apr. 2018.
[112] P. Wang, A. Cavallini, and G. C. Montanari, "The influence of repetitive square wave voltage parameters on enameled wire endurance," *IEEE Trans. Dielectr. Electr. Insul.*, vol. 21, no. 3, pp. 1276–1284, Jun. 2014.
[113] T. Kaji, H. Asai, H. Kojima, and N. Hayakawa, "Combined effect of temperature and humidity of magnet-wires on partial discharge inception voltage under inverter-surge voltage," in *Proc. IEEE Conf. Electr. Insul. Dielectr. Phenomena (CEIDP)*, Oct. 2018, pp. 554–557.
[114] L. Lusuardi, A. Cavallini, M. G. de la Calle, J. M. Martinez-Tarifa, and G. Robles, "Insulation design of low voltage electrical motors fed by PWM inverters," *IEEE Elect. Insul. Mag.*, vol. 35, no. 3, pp. 7–15, May 2019.
[115] V. Madonna, P. Giangrande, W. Zhao, H. Zhang, C. Gerada, and M. Galea, "Electrical machines for the more electric aircraft: Partial discharges investigation," *IEEE Trans. Ind. Appl.*, vol. 57, no. 2, pp. 1389–1398, Dec. 2021.
[116] A. Rumi, J. Marinelli, and A. Cavallini, "Towards the 2nd edition of IEC 60034-18-41: Challenges and perspectives," in *Proc. 3rd Int. Conf. High Voltage Eng. Power Syst. (ICHVEPS)*, Oct. 2021, pp. 52–56.
[117] V. Madonna, P. Giangrande, and M. Galea, "Evaluation of strand-to-strand capacitance and dissipation factor in thermally aged enamelled coils for low-voltage electrical machines," *IET Sci., Meas. Technol.*, vol. 13, no. 8, pp. 1170–1177, Oct. 2019.
[118] S. Savin, S. Ait-Amar, and D. Roger, "Turn-to-turn capacitance variations correlated to PDIV for AC motors monitoring," *IEEE Trans. Dielectr. Electr. Insul.*, vol. 20, no. 1, pp. 34–41, Feb. 2013.
[119] Z. Huang, "Modeling and testing of insulation degradation due to dynamic thermal loading of electrical machines," Ph.D. dissertation, Ind. Electr. Eng. Automat., Lund, Sweden, 2017.
[120] K. N. Gyftakis, M. Sumislawska, D. F. Kavanagh, D. A. Howey, and M. McCulloch, "Dielectric characteristics of electric vehicle traction motor winding insulation under thermal ageing," in *Proc. IEEE 15th Int. Conf. Environ. Electr. Eng. (EEEIC)*, Jun. 2015, pp. 313–318.
[121] M. Farahani, E. Gockenbach, H. Borsi, K. Schäfer, and M. Kaufhold, "Behavior of machine insulation systems subjected to accelerated thermal aging test," *IEEE Trans. Dielectr. Electr. Insul.*, vol. 17, no. 5, pp. 1364–1372, Oct. 2010.
[122] K. N. Gyftakis, P. A. Panagiotou, N. Lophitis, D. A. Howey, and M. D. McCulloch, "Breakdown resistance analysis of traction motor winding insulation under thermal ageing," in *Proc. IEEE Energy Convers. Congr. Expo. (ECCE)*, Oct. 2017, pp. 5819–5825.
[123] G. C. Montanari and P. Seri, "About the definition of PDIV and RPDIV in designing insulation systems for rotating machines controlled by inverters," in *Proc. IEEE Electr. Insul. Conf. (EIC)*, Jun. 2018, pp. 554–557.
[124] G. C. Montanari, P. Seri, and R. Hebner, "Type of supply waveform, partial discharge behavior and life of rotating machine insulation systems," in *Proc. IEEE Int. Power Modulator High Voltage Conf. (IPMHVC)*, Jun. 2018, pp. 176–179.
[125] L. Lusuardi, A. Cavallini, A. Caprara, F. Bardelli, and A. Cattazzo, "The impact of test voltage waveform in determining the repetitive partial discharge inception voltage of type I turn/turn insulation used in inverter-fed induction motors," in *Proc. IEEE Electr. Insul. Conf. (EIC)*, Jun. 2018, pp. 478–481.
[126] J. L. Parpal, J. P. Crine, and C. Dang, "Electrical aging of extruded dielectric cables. A physical model," *IEEE Trans. Dielectr. Electr. Insul.*, vol. 4, no. 2, pp. 197–209, Apr. 1997.
[127] J.-P. Crine, "On the interpretation of some electrical aging and relaxation phenomena in solid dielectrics," *IEEE Trans. Dielectr. Electr. Insul.*, vol. 12, no. 6, pp. 1089–1107, Dec. 2005.
[128] L. V. Hanisch and M. Henke, "Lifetime modelling of electrical machines using the methodology of design of experiments," in *Proc. Symp. Simulationstechnik (ASIM SST)*. Vienna, Austria: ARGESIM Publisher Vienna, 2020, pp. 319–325.
[129] P. Cygan and J. R. Laghari, "Models for insulation aging under electrical and thermal multistress," *IEEE Trans. Electr. Insul.*, vol. 25, no. 5, pp. 923–934, Oct. 1990.
[130] V. N. Höpner and V. E. Wilhelm, "Insulation life span of low-voltage electric motors—A survey," *Energies*, vol. 14, no. 6, p. 1738, Mar. 2021.
[131] S. Arrhenius, "Über die dissociationswärme und den einfluss der temperatur auf den dissociationsgrad der elektrolyte," *Z. Phys. Chem.*, vol. 4, no. 1, pp. 96–116, 1889.
[132] T. W. Dakin, "Electrical insulation deterioration treated as a chemical rate phenomenon," *Trans. Amer. Inst. Electr. Eng.*, vol. 67, no. 1, pp. 113–122, Jan. 1948.
[133] *Test Procedure for the Determination of the Temperature Index of Enamelled and Tape Wrapped Winding Wires*, Standard IEC 60172, 2021.

[134] G. C. Montanari, "Time behavior of partial discharges and life of type II turn insulation specimens under repetitive impulse and sinusoidal waveforms," *IEEE Elect. Insul. Mag.*, vol. 33, no. 6, pp. 17–26, Nov. 2017.

[135] W. Hauschild and W. Mosch, *Statistical Techniques for High-Voltage Engineering* (IEE Power Series), vol. 13. Edison, NJ, USA: IET, 1992.

[136] *Guide for the Statistical Analysis of Electrical Insulation Breakdown Data*, Standard IEC 62539, 2004.

[137] A. Caprara, G. Ciotti, A. Cavallini, and A. Rumi, "The RPDIV and the limits of its definition according to IEC 60034-18-41: The effect of voltage conditioning," in *Proc. IEEE Electr. Insul. Conf. (EIC)*, Jun. 2019, pp. 180–183.

[138] *Rotating Electrical Machines—Part 18–42: Partial Discharge Resistant Electrical Insulation Systems (Type II) Used in Rotating Electrical Machines Fed From Voltage Converters—Qualification Tests*, Standard IEC 60034-18-42, 2020.

[139] *Rotating Electrical Machines—Part 18–21: Functional Evaluation of Insulation Systems—Test Procedures for Wire-Wound Windings—Thermal Evaluation and Classification*, Standard IEC 60034-18-21, 2013.

[140] *Rotating Electrical Machines—Part 18–31: Functional Evaluation of Insulation Systems—Test Procedures for Form-Wound Windings—Thermal Evaluation and Classification of Insulation Systems Used in Rotating Machines*, Standard IEC 60034-18-31, 2012.

[141] *Rotating Electrical Machines—Part 18–1: Functional Evaluation of Insulation Systems—General Guidelines*, Standard IEC 60034-18-1, 2020.

[142] S. Grubic, J. M. Aller, B. Lu, and T. G. Habetler, "A survey on testing and monitoring methods for stator insulation systems of low-voltage induction machines focusing on turn insulation problems," *IEEE Trans. Ind. Electron.*, vol. 55, no. 12, pp. 4127–4136, Dec. 2008.

[143] M. Denk and M. M. Bakran, "Partial discharge measurement in a motor winding fed by a SiC inverter—How critical is high dV/dt really?" in *Proc. PCIM Eur.*, 2018, pp. 685–690.

[144] F. Loubeau, "Analyse des phénomènes de vieillissement des matériaux d'isolation électrique de machines de traction électrique," Ph.D. dissertation, Laboratoire de Génie Electrique de Grenoble (G2Elab), Universite Grenoble Alpes, Grenoble, France, 2017.

[145] P. Giangrande, V. Madonna, S. Nuzzo, and M. Galea, "Moving toward a reliability-oriented design approach of low-voltage electrical machines by including insulation thermal aging considerations," *IEEE Trans. Transport. Electrific.*, vol. 6, no. 1, pp. 16–27, Mar. 2020.

[146] S. B. Lee, A. Naeini, S. Jayaram, G. C. Stone, and M. Sasic, "Surge test-based identification of stator insulation component with partial discharge activity for low voltage AC motors," *IEEE Trans. Ind. Appl.*, vol. 56, no. 3, pp. 2541–2549, May 2020.

[147] T. Hammarström, "Partial discharges at fast rising voltages," Ph.D. dissertation, High Voltage Eng., Chalmers Univ. Technol., Gothenburg, Sweden, 2014.

[148] T. Billard, T. Lebey, and F. Fresnet, "Partial discharge in electric motor fed by a PWM inverter: Off-line and on-line detection," *IEEE Trans. Dielectr. Electr. Insul.*, vol. 21, no. 3, pp. 1235–1242, Jun. 2014.

[149] *Rotating Electrical Machines—Part 18–32: Functional Evaluation of Insulation Systems—Test Procedures for Form-Wound Windings—Evaluation by Electrical Endurance*, Standard IEC 60034-18-32, 2020.

[150] F. Álvarez, F. Garnacho, J. Ortego, and M. Á. Sánchez-Urán, "Application of HFCT and UHF sensors in On-line partial discharge measurements for insulation diagnosis of high voltage equipment," *Sensors*, vol. 15, no. 4, pp. 7360–7387, Apr. 2015.

[151] W. Min, H. Cao, J. Cao, H.-L. Nguyen, J. B. Gomes, and S. P. Krishnaswamy, "An overview of state-of-the-art partial discharge analysis techniques for condition monitoring," *IEEE Electr. Insul. Mag.*, vol. 31, no. 6, pp. 22–35, Nov./Dec. 2015.

[152] L. Niemeyer, "A generalized approach to partial discharge modeling," *IEEE Trans. Dielectr. Electr. Insul.*, vol. 2, no. 4, pp. 510–528, Aug. 1995.

[153] H. Xiong, R. Liu, B. Hu, H. You, Z. Wei, J. Zhang, and J. Wang, "The Ohio State University partial discharge detection platform for electric machine windings driven by PWM voltage excitation," in *Proc. IEEE Electr. Insul. Conf. (EIC)*, Jun. 2019, pp. 517–520.

[154] R. Bozzo and F. Guastavino, "PD detection and localization by means of acoustic measurements on hydrogenerator stator bars," *IEEE Trans. Dielectr. Electr. Insul.*, vol. 2, no. 4, pp. 660–666, Aug. 1995.

[155] S. Coenen and S. Tenbohlen, "Location of PD sources in power transformers by UHF and acoustic measurements," *IEEE Trans. Dielectr. Electr. Insul.*, vol. 19, no. 6, pp. 1934–1940, Dec. 2012.

[156] M. Szczepanski, D. Malec, P. Maussion, B. Petitgas, and P. Manfe, "Ozone concentration impact on the lifespan of enameled wires (conventional and corona-resistant) for low voltage rotating machines fed by inverters," in *Proc. IEEE Electr. Insul. Conf. (EIC)*, Jun. 2017, pp. 443–446.

[157] *High-Voltage Test Techniques—Partial Discharge Measurements*, Standard IEC 60270, 2016.

[158] C. Hudon and M. Belec, "Partial discharge signal interpretation for generator diagnostics," *IEEE Trans. Dielectr. Electr. Insul.*, vol. 12, no. 2, pp. 297–319, Apr. 2005.

[159] E. Gulski, "Digital analysis of partial discharges," *IEEE Trans. Dielectr. Electr. Insul.*, vol. 2, no. 5, pp. 822–837, Oct. 1995.

[160] W. Koltunowicz and R. Plath, "Synchronous multi-channel PD measurements," *IEEE Trans. Dielectr. Electr. Insul.*, vol. 15, no. 6, pp. 1715–1723, Dec. 2008.

[161] B. Gorgan, W. Koltunowicz, and P. Zander, "Temporary monitoring of stator winding insulation using an advanced PD system," in *Proc. Int. Conf. Diag. Electr. Eng. (Diagnostika)*, Sep. 2020, pp. 1–4.

[162] *Electrical Insulating Materials and Systems—Electrical Measurement of Partial Discharges (PD) Under Short Rise Time and Repetitive Voltage Impulses*, Standard IEC/TS 61934, 2011.

TIMO PETRI was born in Kreuztal, Germany, in January 1997. He received the B.Sc. and M.Sc. degrees in electrical engineering from the University of Siegen, Germany, in 2018 and 2020, respectively. He is currently pursuing the joint Ph.D. degree in electrical engineering with the University of Stuttgart, Germany, in cooperation with Robert Bosch GmbH, Renningen, Germany. His research interests include insulation resilience and design of automotive traction machines.

MARINA KELLER was born in Künzelsau, Germany. She received the degree in electrical engineering from the University of Stuttgart, in 2011, where she is currently pursuing the Ph.D. degree. Afterwards, she worked as a Research Associate at the Institute of Electrical Energy Conversion, University of Stuttgart. Since September 2017, she has been working as a Research Engineer with the Corporate Research Department, Robert Bosch GmbH. Her research interests include modeling and designing electric machines, with a special focus on insulation stress and resilience of traction motor windings.

NEJILA PARSPOUR received the master's degree in electrical engineering and the Ph.D. degree *(summa cum laude)* from the Technical University of Berlin, in 1991 and 1995, respectively. She gained five years of industrial experience at Philips and six years of scientific experience at the University of Bremen. She is currently a Professor in electrical energy conversion at the University of Stuttgart and the Head of the Institute of Electrical Energy Conversion. Her research interests include electrical machines and drives, with a focus on machine design and contactless energy transfer, with a focus on inductive charging systems.